

# Quasi-Monte Carlo for Efficient Fourier Pricing of Multi-Asset Options

Christian Bayer<sup>1</sup>, Chiheb Ben Hammouda<sup>2</sup>, Antonis Papapantoleon<sup>3</sup>, Michael Samet<sup>\*4</sup> and Raúl Tempone<sup>4,5</sup>

<sup>1</sup>Weierstrass Institute for Applied Analysis and Stochastics (WIAS), Berlin, Germany.

<sup>2</sup>Mathematical Institute, Utrecht University, Utrecht, the Netherlands

<sup>3</sup>Delft Institute of Applied Mathematics, EEMCS, TU Delft, 2628 Delft, The Netherlands, and Department of Mathematics, SAMPS, NTUA, 15780 Athens, Greece and Institute of Applied and Computational Mathematics, FORTH, 70013 Heraklion, Greece.

<sup>4</sup>Chair of Mathematics for Uncertainty Quantification, RWTH Aachen University, Aachen, Germany.

<sup>5</sup>King Abdullah University of Science and Technology (KAUST), Computer, Electrical and Mathematical Sciences & Engineering Division (CEMSE), Thuwal, Saudi Arabia.

## Abstract

Efficiently pricing multi-asset options poses a significant challenge in quantitative finance. The Monte Carlo (MC) method remains the prevalent choice for pricing engines; however, its slow convergence rate impedes its practical application. Fourier methods leverage the knowledge of the characteristic function to accurately and rapidly value options with up to two assets. Nevertheless, they face hurdles in the high-dimensional settings due to the tensor product (TP) structure of commonly employed quadrature techniques. This work advocates using the randomized quasi-MC (RQMC) quadrature to improve the scalability of Fourier methods with high dimensions. The RQMC technique benefits from the smoothness of the integrand and alleviates the curse of dimensionality while providing practical error estimates. Nonetheless, the applicability of RQMC on the unbounded domain,  $\mathbb{R}^d$ , requires a domain transformation to  $[0, 1]^d$ , which may result in singularities of the transformed integrand at the corners of the hypercube, and deteriorate the rate of convergence of RQMC. To circumvent this difficulty, we design an efficient domain transformation procedure based on the derived boundary growth conditions of the integrand. This transformation preserves the sufficient regularity of the integrand and hence improves the rate of convergence of RQMC. To validate this analysis, we demonstrate the efficiency of employing RQMC with an appropriate transformation to evaluate options in the Fourier space for various pricing models, payoffs, and dimensions. Finally, we highlight the computational advantage of applying RQMC over MC or TP in the Fourier domain, and over MC in the physical domain for options with up to 15 assets.

**Keywords** option pricing, Fourier methods, quasi-Monte Carlo, multi-asset options, domain transformation, boundary growth conditions

**2010 Mathematics Subject Classification** 65D32, 65T50, 65Y20, 91B25, 91G20, 91G60

---

\*samet@uq.rwth-aachen.de

# 1 Introduction

The computation of the price of options depending on multiple assets presents a long-standing challenge in quantitative finance. European option pricing approaches can be broadly divided into two primary classes. The first class consists of partial differential equation (PDE) approaches, which are typically solved using finite difference, finite volume or finite element methods [15, 60, 19]. Despite the wide literature on the PDE approaches, they tend to suffer from the curse of dimensionality and, hence, are not accommodating for multi-asset option pricing. Recent studies have employed deep learning techniques to address the curse of dimensionality [23, 22, 20]; although the developed methods are efficient, they often rely on computationally intensive offline training procedure. The second class of methods is based on the martingale representation under which the option prices are given as expectations [45]. These expectations can be computed via either stochastic integration methods or deterministic quadrature methods. A commonly applied stochastic integration method is the Monte Carlo (MC) method [21]. The advantage of employing the MC method for multidimensional option pricing is that it yields a dimension-independent convergence rate,  $\mathcal{O}(N^{-\frac{1}{2}})$ , with  $N$  being the number of simulated paths. However, this rate is considered to be prohibitively slow for practical use, especially for model calibration purposes. Deterministic quadrature methods such as quasi-MC (QMC) [14] or (adaptive) sparse grid quadrature (SGQ) [28] methods, can achieve a better rate of convergence than the MC method; however, their rates are sensitive to the dimensionality (the number of underlying assets) and the regularity of the integrand. Moreover, the payoff function, typically exhibits jumps or kinks that deteriorate the performance of deterministic quadrature methods, such as the SGQ and QMC methods. Consequently, considerable research has been devoted to developing analytical and numerical smoothing techniques. For instance, analytical smoothing can be performed by applying a conditional expectation with respect to selected integration variables, as in [63, 8, 6]. However, when these techniques are inapplicable, numerical smoothing can be performed by combining root-finding methods with preintegration [7]. A more implicit smoothing technique is to map the integration problem from the direct space to an image space via an integral transform (e.g., Fourier, Laplace, Mellin, or Hilbert) [42, 54, 19, 53], where the integrand is more regular, or possibly analytic in some region of the complex plane. The integration problem can then be solved more efficiently in the image space if appropriate numerical methods are employed, and a suitable contour of integration is chosen (for more details, see [9, 46, 41]). When the asset log-price process follows complex dynamics and the characteristic function is analytically known, Fourier methods represent a solid alternative to the MC method and PDE approaches for options with up to two underlying assets [56, 33, 11, 30, 59].

The literature on Fourier pricing comprises three main approaches, which we briefly describe (for a more elaborate discussion, refer to the introduction in [9]). The first approach [10] takes the Fourier transform of the exponentially dampened option price with respect to the log-strike variable and applies the fast Fourier transform algorithm to evaluate options for multiple strikes simultaneously. The second approach is known as the COS method [18] and is based on expanding the density function of the log-price in a Fourier cosine series. The third approach takes the inverse extended Fourier transform<sup>1</sup> [16] of the payoff function and the density function separately in the log-price variable. This approach was concurrently interpreted in terms of the double Laplace transform by Raible [54] and the extended Fourier transform by Lewis [42]. The main advantage

---

<sup>1</sup>The extended Fourier transform is sometimes referred to as the Fourier–Laplace transform [16] or the generalized Fourier transform [58].

of the latter approach is that it can be straightforwardly extended to multiple dimensions (for a rigorous analysis in the multiasset setting, refer to [17]). For instance, Hurd and Zhou [30] adopted this approach and proposed a numerical scheme based on the fast Fourier transform for the pricing of two-dimensional (2D) spread options. While their method demonstrated efficiency in handling 2D options, due to its tensor product (TP) nature, the curse of dimensionality occurs for higher-dimensional cases. Bayer et al. [9] demonstrate that the curse of dimensionality can be alleviated by employing a dimension-adaptive sparse grid quadrature method and by parametrically smoothing the integrand via an optimized choice of the contour of integration. Their numerical results show that basket and rainbow options with up to six underlying assets with Lévy dynamics can be priced very efficiently. Other related work [31] uses the tensor-train cross algorithm to exploit the possibly low rank structure of the integrand in the Fourier domain. Nevertheless, this Tensor-Fourier method was reported to become numerically unstable in high dimensions, and the numerical experiments were restricted to the geometric Brownian motion (GBM) model. Thus, only a limited number of studies have offered efficient numerical methodologies for Fourier pricing of multiasset options.

Despite the broad applicability of the randomized QMC (RQMC) method in the direct space, to the best of our knowledge, there have been no attempts to apply the RQMC in the Fourier domain. Early studies treated RQMC on an unbounded domain in the physical space [37, 36]. A well-established result states that, under appropriate smoothness conditions, the RQMC method has a rate of convergence of  $\mathcal{O}(N^{-1+\epsilon_r})$ ,  $\epsilon_r > 0$ , where  $N$  is the number of QMC points and  $\epsilon_r$  depends on the integrand regularity and the problem dimensionality [52]. We aim to exploit knowledge of the analyticity of the integrand to apply the RQMC quadrature to mitigate the curse of dimensionality. We refer to a previous study [9] for a nearly optimal rule to shift the integration contour, accelerating the convergence of quadrature techniques. However, QMC constructions are designed to sample low-discrepancy points on the domain  $[0, 1]^d$ ; hence, an appropriate integral transformation must be performed to address the target Fourier integrand supported on  $\mathbb{R}^d$ . The standard mapping used in the literature to achieve this transformation applies the inverse cumulative distribution function (ICDF), with the caveat that this variable change typically results in a spikier transformed integrand, possibly unbounded near the boundaries of  $[0, 1]^d$ , as noted in [52]. Even if the original integrand is a bounded variation in the sense of Hardy and Krause [51], the transformed integrand may be singular; therefore, the optimal error rate of RQMC is no longer guaranteed. However, in [52], the author proved that the error rate of  $\mathcal{O}(N^{-1+\epsilon_r})$  can be retained under specific "QMC-friendly" growth conditions on the integrand and its derivatives, coupled with conditions on the corner avoidance property of the sample points (for more details, see [24]).

More recently, for functions with a specific exponential rate of growth, RQMC aided by the appropriate importance sampling (IS) technique can achieve the rate of  $\mathcal{O}(N^{-\frac{3}{2}+\epsilon_r})$  [50] (for a study on nonasymptotic convergence rates of RQMC combined with IS, refer to [44]). In contrast to the mentioned research, this integration problem in the Fourier space is deterministic. Consequently, IS is enrooted in the proposed approach, and the choice of the proposal IS density may have adverse effects on the of RQMC. The contributions of this paper are as follows:

- To the best of our knowledge, we are the first to propose the use of RQMC in the Fourier space for option pricing with high dimensions. We provide a practical model-specific domain transformation strategy that avoids introducing the singularity of the integrand near the boundaries of  $[0, 1]^d$ . The key idea is to preserve the original features of the integrand by choosing a proposal domain transformation distribution that asymptotically shares the same

functional form as the extended characteristic function of the pricing dynamics. Then, we tune the parameters of the proposal density to satisfy the derived boundary growth conditions that ensure nearly optimal convergence rates.

- Compared to previous related works [37, 36, 50], we do not treat weighted integration problems with respect to the Gaussian density. We consider more challenging integrands that may have a slower decay (e.g., root-exponential decay in the case of the normal inverse Gaussian (NIG) model and power-law decay in the case of the variance gamma (VG) model). In addition, many researchers have assumed an independent structure exists, allowing them to evaluate the ICDF componentwise using the univariate ICDF. This work proposes a domain transformation that relaxes this assumption, allowing the maneuver of the computation of the ICDF, which is not given in closed-form for most multivariate distributions. The aim is to express the  $d$ -dimensional vector of log-price asset processes in a normal mixture form and use the eigenvalue or Cholesky decomposition to eliminate the dependence between the random variables (RV).
- We demonstrate the computational advantage of employing RQMC in the Fourier space compared to the TP-Laguerre quadrature or MC method in the Fourier space and compared to the MC method in the direct space. We provide several numerical experiments for various pricing models and options with up to 15 underlying assets.

The outline of this paper is as follows. Section 2 introduces the problem setting of multivariate Fourier pricing and provides the necessary background on the RQMC method. In Section 3, we explain our methodology. In Section 3.1, we motivate the importance of appropriately handling the domain transformation to obtain nearly optimal convergence rates of the RQMC method. Then, in Section 3.2, we present practical domain transformation strategies for the GBM, the VG and the NIG models, based on derived boundary growth conditions, summarized in Tables 3.3 and 3.4. Finally, in Section 4, we report and analyze the obtained numerical results. We illustrate the advantages of the proposed domain transformation on the rate of convergence of the RQMC method. Furthermore, we highlight the considerable computational gains achieved compared the TP-Laguerre quadrature and MC method in the Fourier space and compared to the MC method in the physical space, for options with up to 15 assets.

## 2 Problem Setting and Background

Section 2.1 briefly revisits the general Fourier valuation framework for multi-asset options considered in this work (explained in more detail in a previous study [9]). Then, Section 2.2 describes the RQMC method.

### 2.1 Fourier Valuation Formula

The aim is to efficiently compute the price of European options when the asset price follows a multivariate stochastic model (e.g., a Lévy model). To accomplish this aim, we used the multivariate representation of the option price in the Fourier domain, as in previous work [9, 17]. Prior to presenting the valuation formula in Proposition 2.4, we introduce the necessary notation, definitions, and assumptions.

**Notation 2.1** (Notations and Definitions).

- $\mathbf{X}_T := (X_T^1, \dots, X_T^d)$  is a  $d$ -dimensional ( $d \in \mathbb{N}$ ) vector of log-asset prices<sup>2</sup> at a maturity time of  $T > 0$ , whose dynamics follow a multivariate stochastic model with the parameters denoted by the vector  $\Theta_m$ .
- $\Phi_{\mathbf{X}_T}(\mathbf{z}) := \mathbb{E}[e^{i\mathbf{z}'\mathbf{X}_T}]$ , for  $\mathbf{z} \in \mathbb{C}^d$ , denotes the extended characteristic function, where  $\mathbf{z}'$  represents the transpose of  $\mathbf{z}$ . We define the inner product  $\mathbf{x}'\mathbf{y} = \sum_{j=1}^d x_j y_j$  for  $\mathbf{x}, \mathbf{y} \in \mathbb{C}^d$ .
- $P(\mathbf{x})$ ,  $\forall \mathbf{x} \in \mathbb{R}^d$  denotes the payoff function, and  $\widehat{P}(\mathbf{z}) := \int_{\mathbb{R}^d} e^{i\mathbf{z}'\mathbf{x}} P(\mathbf{x}) d\mathbf{x}$ , for  $\mathbf{z} \in \mathbb{C}^d$  represents the extended Fourier transform.
- $\Theta_p = (K, T, r)$  represents the vector of the payoff and market parameters, where  $K$  denotes the strike price, and  $r$  is the risk-free interest rate.
- $i$  denotes the unit imaginary number, and  $\Re[\cdot]$  and  $\Im[\cdot]$  represent the real and imaginary parts of a complex number, respectively.
- $L_{bc}^1(\mathbb{R}^d)$  denotes the space of bounded and continuous functions in  $L^1(\mathbb{R}^d)$ .
- $\mathbf{A} \in \mathbb{R}^{d \times d}$  is a matrix. In addition,  $\mathbf{A} \succ 0$  (respectively  $\mathbf{A} \succeq 0$ ) denotes positive (semi-)definiteness, and  $\mathbf{A} \prec 0$  (respectively  $\mathbf{A} \preceq 0$ ) denotes the negative (semi-)definiteness of matrix  $\mathbf{A}$ .
- Let  $\mathbb{I}_d := \{1, \dots, d\}$ .

**Assumption 2.2** (Assumptions on the payoff).

1. There exists  $\mathbf{R} \in \delta_P := \{\mathbf{R} \in \mathbb{R}^d \mid \mathbf{x} \mapsto e^{-\langle \mathbf{R}, \mathbf{x} \rangle} P(\mathbf{x}) \in L_{bc}^1(\mathbb{R}^d) \text{ and } \mathbf{y} \mapsto \widehat{P}(\mathbf{y} + i\mathbf{R}) \in L^1(\mathbb{R}^d)\}$ .

**Assumption 2.3** (Assumption on the Corresponding Characteristic Function).

1. There exists  $\mathbf{R} \in \delta_X := \{\mathbf{R} \in \mathbb{R}^d \mid |\mathbf{y} \mapsto \Phi_{\mathbf{X}_T}(\mathbf{y} + i\mathbf{R})| < \infty, \forall \mathbf{y} \in \mathbb{R}^d\}$ .

**Proposition 2.4** (Multivariate Fourier Pricing Valuation Formula). *We employ the notation in 2.1 and suppose that Assumptions 2.2 and 2.3 hold and that  $\delta_V = \delta_X \cap \delta_P \neq \emptyset$ . Then, for  $\mathbf{R} \in \delta_V$ , the option value is given by the following:*

$$(2.1) \quad V(\Theta_m, \Theta_p) = (2\pi)^{-d} e^{-rT} \Re \left( \int_{\mathbb{R}^d} \Phi_{\mathbf{X}_T}(\mathbf{y} + i\mathbf{R}) \widehat{P}(\mathbf{y} + i\mathbf{R}) d\mathbf{y} \right).$$

*Proof.* For proof of Proposition 2.4, refer to [9]. □

From (2.1), we define the integrand of interest as follows:

$$(2.2) \quad g(\mathbf{y}; \mathbf{R}, \Theta_m, \Theta_p) := (2\pi)^{-d} e^{-rT} \Re[\Phi_{\mathbf{X}_T}(\mathbf{y} + i\mathbf{R}) \widehat{P}(\mathbf{y} + i\mathbf{R})], \mathbf{y} \in \mathbb{R}^d, \mathbf{R} \in \delta_V.$$

The integrand in (2.2) is analytic along the horizontal lines, and  $\mathbf{z} = \mathbf{y} + i\mathbf{R} \in \mathbb{R}^d + i\delta_V \subseteq \mathbb{C}^d$ . This observation motivates the use of quadrature methods that leverage the analyticity to enhance the

---

<sup>2</sup>  $X_T^i := \log(S_T^i)$ ,  $i = 1, \dots, d$ ,  $\{S_T^i\}_{i=1}^d$  are asset prices at maturity  $T$ .

convergence rates compared to traditional approaches, such as the MC method [9]. In addition, we suggest the use of the RQMC quadrature in the Fourier space to address the integration problem efficiently in high dimensions. Section 2.2 introduces the RQMC method, and Section 3 explains the necessary transformations to implement the RQMC method in the Fourier setting. Next, Section 4 presents the benefits of adopting this approach through concrete examples involving basket and rainbow options under various pricing models.

## 2.2 RQMC Method

This section introduces the RQMC method. When the integral of a function  $g(\cdot)$  is computed over  $[0, 1]^d$ , the QMC estimator denoted by  $Q_{N,d}^{QMC}[\cdot]$  is an  $N$ -point equal-weighted quadrature rule:

$$(2.3) \quad I[g] := \int_{[0,1]^d} g(\mathbf{y}) d\mathbf{y} \approx Q_{N,d}^{QMC}[g] := \frac{1}{N} \sum_{n=1}^N g(\mathbf{u}_n),$$

where  $\mathbf{u}_1, \dots, \mathbf{u}_N$  is a set of deterministic low-discrepancy points (e.g., Sobol, Niederreiter, Halton, Hammersley, and Faure [57, 38, 62])  $\mathbf{u}_n \in [0, 1]^d, n \in \{1, \dots, N\}$ . The advantage of (2.3) compared to the MC estimator is that the points  $\{\mathbf{u}_n\}_{n=1}^N$  are generated to ensure the more uniform coverage of  $[0, 1]^d$ . Consequently, the estimator (2.3) may achieve a convergence rate of order  $\mathcal{O}(N^{-1+\epsilon_r})$  [52], with  $\epsilon_r > 0$ , depending on the regularity of  $g(\cdot)$  and the dimension,  $d$ , of the domain. In contrast, MC points are sampled randomly and independently and may cluster and miss important regions of the integrand unless IS techniques are employed [21]. Nonetheless, the shortcoming of the estimator in (2.3) is that the central limit theorem cannot be directly applied to obtain probabilistic error estimates as in the case of the MC method. The points  $\{\mathbf{u}_n\}_{n=1}^N$  are not sampled independently. In [27], a deterministic error bound for the estimator in (2.3) was derived, known as the Koksma–Hlawka inequality [27]. This error bound is commonly impractical because its computation involves the integration of the mixed first partial derivatives of the integrand, which is commonly more difficult than solving the original problem. As a remedy, a randomized variant of the QMC estimator (2.3) was introduced (see [40]), called the RQMC estimator, given by

$$(2.4) \quad Q_{N,S,d}^{RQMC}[g] := \frac{1}{S} \sum_{s=1}^S \frac{1}{N} \sum_{n=1}^N g(\mathbf{u}_n^{(s)}),$$

where  $\{\mathbf{u}_n\}_{n=1}^N$  is the sequence of deterministic QMC points, and for  $n = 1, \dots, N$ ,  $\{\mathbf{u}_n^{(s)}\}_{s=1}^S$  is obtained by the appropriate randomization of  $\{\mathbf{u}_n\}_{n=1}^N$ , such that  $\mathbf{u}_n^{(s)} \sim \mathcal{U}([0, 1]^d)$ . For fixed  $n = 1, \dots, N$ ,  $\mathbf{u}_n^{(s)}$  are independent  $\forall s = 1, \dots, S$ . An additional rationale to apply the RQMC estimator is that the set of points  $\{\mathbf{u}_n^{(s)}\}_{s=1}^S$  yields an unbiased estimator (2.4) (i.e.,  $\mathbb{E}[Q_{N,S,d}^{RQMC}[g]] = I[g]$ ). Several randomization methods exist with different theoretical guarantees (for an overview of the most popular methods, see [40]). This work adopts Sobol sequences with digital shift. Finally, the randomization of the low-discrepancy points enables the derivation of the root mean squared error of the estimator, given by

$$(2.5) \quad \mathcal{E}_{N,S,d}^{RQMC} := \frac{C_\alpha}{\sqrt{S}} \sqrt{\frac{1}{S-1} \sum_{s=1}^S \left( \frac{1}{N} \sum_{n=1}^N g(\mathbf{u}_n^{(s)}) - Q_{N,d}^{RQMC}[g] \right)^2},$$

where  $C_\alpha$  denotes the  $(1 - \frac{\alpha}{2})$ -quantile of the standard normal distribution for a confidence level  $0 < \alpha \ll 1$ . In this work,  $C_\alpha = 1.96$  for  $\alpha = 0.05$ . Moreover, (2.5) reveals that the statistical error can be controlled by the number of shifts,  $S$ , which we apply in the order of  $S = 30$  to achieve a reliable error estimate.

Despite the advantages of using RQMC to obtain easily computable error estimates, this method suffers from a significant drawback, which may impede its application, especially for high-dimensional problems. Specifically, the construction of QMC points is constrained to simple geometries, such as the hypercube,  $[0, 1]^d$ ; hence, transformations of the original domains to the hypercube are necessary to address unbounded integrals in the form of (2.1), as we discuss in Section 3.

### 3 Efficient Domain Transformation for RQMC in Fourier Pricing

This section explains how the RQMC estimator in (2.4) can be applied to the Fourier integral defined on  $\mathbb{R}^d$ . Section 3.1 details the general approach to transforming the pricing problem defined in Proposition 2.4. Section 3.2 proposes a strategy to manage the domain transformation efficiently for three models: GBM, VG, and NIG.

#### 3.1 General Formulation

The main QMC constructions (for a comprehensive survey, see [40]) are restricted to the generation of low-discrepancy point sets on  $[0, 1]^d$ . Consequently, an appropriate integral transformation is necessary to apply RQMC to a more general domain, such as the unbounded domain,  $\mathbb{R}^d$ . The following mapping is the typical transformation in the literature to map an integrand from  $\mathbb{R}^d$  to  $[0, 1]^d$  [37, 36, 49, 5, 43, 50]:

$$(3.1) \quad \mathbf{u} = \Psi(\mathbf{y}; \mathbf{\Lambda}) \Leftrightarrow \mathbf{y} = \Psi^{-1}(\mathbf{u}; \mathbf{\Lambda}), \mathbf{u} \in [0, 1]^d,$$

where  $\mathbf{u} \mapsto \Psi(\mathbf{u}; \mathbf{\Lambda})$  is the cumulative distribution function (CDF) of some  $\mathbb{R}^d$ -valued RV with parameter vector  $\mathbf{\Lambda}$  (e.g., mean, scale, and degrees of freedom), and  $\Psi^{-1}(\mathbf{u}; \mathbf{\Lambda})$  is the ICDF.

Other domains, such as spheres or simplices, would require different mappings (for more details, see [5] and the references therein). For the sake of brevity, we omit writing the explicit dependence of  $\Psi^{-1}(\mathbf{u})$  on the parameter vector  $\mathbf{\Lambda}$ . By applying the change in variable in (3.1) to the integral in (2.1), we obtain the following:

$$(3.2) \quad V(\Theta_m, \Theta_p) = \int_{[0, 1]^d} \tilde{g}(\mathbf{u}) d\mathbf{u},$$

$$\tilde{g}(\mathbf{u}) := \frac{g \circ \Psi^{-1}(\mathbf{u})}{\psi \circ \Psi^{-1}(\mathbf{u})}, \quad \mathbf{u} \in [0, 1]^d,$$

where  $g(\cdot)$  is the integrand defined in (2.2), and  $\psi(\cdot)$  denotes the probability density function (PDF) corresponding to  $\Psi(\cdot)$ . The primary challenge of this domain transformation is that it often results in integrands that are unbounded near the boundary [52]. Because  $\lim_{u_j \rightarrow 0} \Psi^{-1}(u_j) = -\infty, j \in \mathbb{I}_d \Rightarrow \lim_{u_j \rightarrow 0} \psi \circ \Psi^{-1}(u_j) \rightarrow 0$ . Through symmetry, the same argument applies when  $u_j \rightarrow 1$ . Consequently, unless the decay of the numerator in (3.2),  $\mathbf{u} \mapsto g \circ \Psi^{-1}(\mathbf{u})$ , is faster than the decay of denominator,  $\mathbf{u} \mapsto \psi \circ \Psi^{-1}(\mathbf{u})$ , the integrand is singular at the boundaries of  $[0, 1]^d$ . Unbounded

integrands do not satisfy the assumptions of the Koksma–Hlawka error bound (i.e., the variation of the integrand in the sense of Hardy and Krause is infinite); thus, the rate of convergence of RQMC may deteriorate. Therefore, finding an appropriate choice of  $\psi(\cdot)$  (respectively  $\Psi^{-1}(\cdot)$ ), such that the transformed integrand  $\tilde{g}(\cdot)$  is sufficiently smooth is critical.

Most of the literature [37, 35, 49, 36, 50] considers the weighted integration problem, which is different from the problem considered in (3.2), which can be written as follows:

$$(3.3) \quad \int_{\mathbb{R}^d} g(\mathbf{y}) \left( \prod_{j=1}^d \rho(y_j) \right) dy_1 \dots dy_d,$$

where  $\rho(\mathbf{y}) = \prod_{j=1}^d \rho(y_j)$  is a joint PDF of independent RVs, a problem characteristically arising when computing  $\mathbb{E}_\rho[g(\mathbf{Y})]$ , with  $\mathbf{Y}$  as a random vector. Applying the change in variable (3.1) to (3.3) results in the following integration problem:

$$(3.4) \quad \int_{\mathbb{R}^d} g(\mathbf{y}) \left( \prod_{j=1}^d \rho(y_j) \right) dy_1 \dots dy_d = \int_{[0,1]^d} g \circ \Psi^{-1}(\mathbf{u}) \left( \prod_{j=1}^d \frac{\rho \circ \Psi^{-1}(u_j)}{\psi \circ \Psi^{-1}(u_j)} \right) du_1 \dots du_d.$$

The computation of the  $\rho$ -weighted integral in (3.4) is more straightforward than the integration problem considered in (3.2) for the following reasons.

- In the proposed framework (3.2), the choice of  $\psi(\cdot)$  is more restrictive than in (3.4). The space of density functions,  $\psi(\cdot)$ , ensuring that  $\frac{g \circ \Psi^{-1}}{\psi \circ \Psi^{-1}} \in L^1(\mathbb{R}^d)$ , is included in the space of densities that enforce that  $\frac{(g\rho) \circ \Psi^{-1}}{\psi \circ \Psi^{-1}} \in L^1(\mathbb{R}^d)$ . The set of candidate densities is considerably larger in the weighted integration setting, especially when  $\rho(\cdot)$  is rapidly decaying (e.g., a Gaussian density).
- The integration problem in (3.3) assumes an independence structure, implying that  $\Psi^{-1}(\mathbf{u}) = (\Psi^{-1}(u_1), \dots, \Psi^{-1}(u_d))$ , where the univariate ICDF is applied componentwise on the right-hand side. However, in financial applications, RVs are commonly dependent, making it challenging to evaluate  $\Psi^{-1}(\mathbf{u})$  numerically for a general multivariate ICDF. Section 3.2 develops a domain transformation strategy to avoid this computation.

Equation (3.4) reveals how this change in variables relates to the IS technique. In the MC method, the density  $\psi(\cdot)$  is set to minimize the variance of the transformed integrand. However, in the proposed setting,  $\psi(\cdot)$  must be chosen more carefully because the performance of RQMC highly depends on the regularity of the integrand (for a more detailed analysis, refer to [25]). In this work, we base the choice of  $\psi(\cdot)$  on the following properties.

- We are interested in densities,  $\psi(\cdot)$  that are smooth; hence,  $\Psi^{-1}(\mathbf{u})$  is smooth in  $(0, 1)^d$  [36].
- We set  $\psi(\cdot)$  as even because the original integrand in (2.2) is even (a consequence of Fourier transform properties).
- We set the density  $\psi(\cdot)$  to follow the same functional form of the extended characteristic function asymptotically. This approach allows the control of the decay of the integrand near the boundary for various model parameters  $(\Theta_m)$  and maturity dates  $(T)$ .

- We selected the parameter  $\Lambda$  of  $\psi(\cdot)$  to control the boundary growth of the transformed integrand in (3.2). We separately derived the boundary growth conditions for each of the pricing models (for more details, see Sections 3.2.1, 3.2.2, and 3.2.1). Table 3.1 presents examples of the characteristic functions considered in this work.

Once the choice of  $\psi(\cdot)$  (respectively  $\Psi^{-1}(\cdot)$ ) is determined, the RQMC estimator of (3.2) can be expressed as follows:

$$Q_{N,S,d}^{RQMC}[\tilde{g}] := \frac{1}{S} \sum_{s=1}^S \frac{1}{N} \sum_{n=1}^N \tilde{g}(\mathbf{u}_n^{(s)}).$$

Model	$\phi_{\mathbf{X}_T}(\mathbf{z})$
GBM	$\exp(\mathbf{iz}'(\mathbf{r} - \frac{1}{2} \text{diag}(\Sigma))T - \frac{T}{2} \mathbf{z}'\Sigma\mathbf{z}), \quad \mathbf{z} \in \mathbb{C}^d, \Im[\mathbf{z}] \in \delta_X$
VG	$\exp(\mathbf{iz}'(\mathbf{r} + \boldsymbol{\mu}_{VG})T) (1 - i\nu\mathbf{z}'\boldsymbol{\theta} + \frac{1}{2}\nu\mathbf{z}'\Sigma\mathbf{z})^{-T/\nu}, \quad \mathbf{z} \in \mathbb{C}^d, \Im[\mathbf{z}] \in \delta_X$
NIG	$\exp\left(\mathbf{iz}'(\mathbf{r} + \boldsymbol{\mu}_{NIG})T + \delta T \left(\sqrt{\alpha^2 - \boldsymbol{\beta}'\Delta\boldsymbol{\beta}} - \sqrt{\alpha^2 - (\boldsymbol{\beta} + \mathbf{iz})'\Delta(\boldsymbol{\beta} + \mathbf{iz})}\right)\right),$ $\mathbf{z} \in \mathbb{C}^d, \Im[\mathbf{z}] \in \delta_X$

Table 3.1: Extended characteristic function given by  $\Phi_{\mathbf{X}_T}(\mathbf{z}) = \exp(\mathbf{iz}'\mathbf{X}_0)\phi_{\mathbf{X}_T}(\mathbf{z})$  for various pricing models.  $\mathbf{r} = (r, \dots, r)$  denotes a  $d$ -dimensional constant vector. Table 3.2 provides the strip of analyticity for each of the pricing models. Appendix A presents more details on the model parameters.

Model	$\delta_X$
GBM	$\mathbb{R}^d$
VG	$\{\mathbf{R} \in \mathbb{R}^d \mid 1 + \nu\mathbf{R}'\boldsymbol{\theta} - \frac{1}{2}\nu\mathbf{R}'\Sigma\mathbf{R} > 0\}$
NIG	$\{\mathbf{R} \in \mathbb{R}^d \mid \alpha^2 - (\boldsymbol{\beta} - \mathbf{R})'\Delta(\boldsymbol{\beta} - \mathbf{R}) > 0\}$

Table 3.2: Strip of analyticity,  $\delta_X$ , of the characteristic functions for the different pricing models.

Figure 3.1 illustrates the importance of efficiently designing the domain transformation procedure. The effect of the parameter  $\tilde{\sigma}$  is visualized in the mapping on the smoothness of the integrand in the case of a 1D put option under the GBM model and is compared to the original integrand on  $\mathbb{R}^d$ . Figure 3.1b indicates that, for  $\tilde{\sigma} = 1$ , the integrand is singular near the boundary, whereas the original integrand in Figure 3.1a is regular. Moreover, for larger values of  $\tilde{\sigma}$ , the integrand decays to zero. Section 3.2.1 clarifies the reason for this decay.

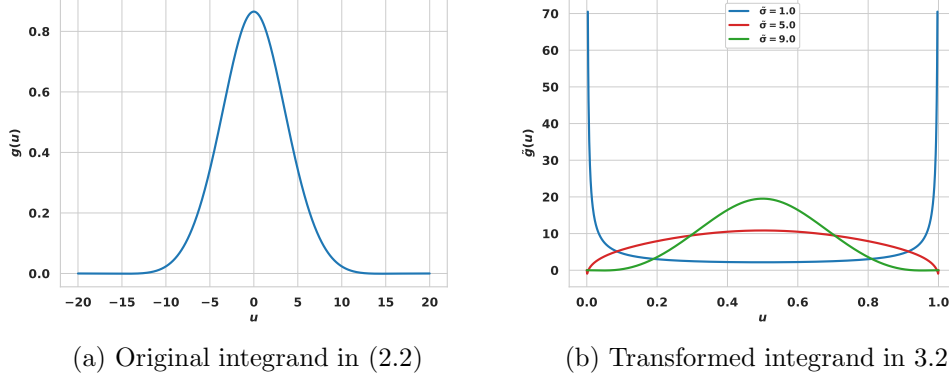


Figure 3.1: Effect of the domain transformation on the smoothness of the transformed integrand (3.2) for a put option under GBM, where  $\sigma = 0.2$ . Gaussian density:  $\psi(\cdot; \tilde{\mu}, \tilde{\sigma})$ , mean:  $\tilde{\mu} = 0$ , standard deviation:  $\tilde{\sigma}$ .

### 3.2 Model-dependent Domain Transformation

In this section, the primary aim is to develop a general domain transformation strategy to apply the RQMC method in the Fourier domain to a wide range of pricing models. We derived the boundary growth conditions for models with different asymptotic decay rates of the characteristic functions,  $\mathcal{O}(\exp(-C \|\mathbf{y}\|^2))$ ,  $\mathcal{O}(\exp(-C \|\mathbf{y}\|))$ , and  $\mathcal{O}((C \|\mathbf{y}\|)^{-\gamma})$ , where  $\mathbf{y} \in \mathbb{R}^d$ ,  $C, \gamma > 0$ . For the sake of concreteness, we considered the GBM, VG, and NIG to be representative examples of different decay rates of characteristic functions. We developed a model-dependent domain transformation strategy to apply the RQMC method in all three models. Section 4 provides several numerical experiments to justify the analysis. This section summarizes by providing the proposed domain transformation strategy for each of the studied models in Tables 3.3 and 3.4. Sections 3.2.1, 3.2.2, and 3.2.3 provide details on the derivation.

Table 3.3: Choice of  $\psi_j(\cdot)$  and conditions on  $\mathbf{\Lambda}$  for (i) GBM, (ii) VG, and (iii) NIG in the case of independent assets.

Model	$\psi_j(y_j; \mathbf{\Lambda})$	Boundary growth condition on $\mathbf{\Lambda}$
GBM	$\frac{1}{\sqrt{2\tilde{\sigma}_j^2}} \exp\left(-\frac{y_j^2}{2\tilde{\sigma}_j^2}\right)$	$\tilde{\sigma}_j \geq \frac{1}{\sqrt{T}\sigma_j}$
VG	$\frac{\Gamma\left(\frac{\tilde{\nu}+1}{2}\right)}{\sqrt{\tilde{\nu}\pi\tilde{\sigma}_j}\Gamma\left(\frac{\tilde{\nu}}{2}\right)} \left(1 + \frac{y_j^2}{\tilde{\nu}\tilde{\sigma}_j^2}\right)^{-(\tilde{\nu}+1)/2}$	$\tilde{\nu} \leq \frac{2T}{\nu} - 1,$ $\tilde{\sigma}_j = \left[\frac{\nu\sigma_j^2\tilde{\nu}}{2}\right]^{\frac{T}{\nu-2T}} (\tilde{\nu})^{\frac{\nu}{4T-2\nu}}$
NIG	$\frac{\exp\left(-\frac{ y_j }{\tilde{\sigma}_j}\right)}{2\tilde{\sigma}_j}$	$\tilde{\sigma}_j \geq \frac{1}{\delta T}$

Table 3.4: Choice of  $\psi(\cdot)$  and conditions on  $\mathbf{\Lambda}$  for (i) GBM, (ii) VG, and (iii) NIG in the case of dependent assets.

Model	$\psi(\mathbf{y}; \mathbf{\Lambda})$	Boundary growth condition on $\mathbf{\Lambda}$
GBM	$(2\pi)^{-\frac{d}{2}} (\det(\tilde{\Sigma}))^{-\frac{1}{2}} \exp\left(-\frac{1}{2}(\mathbf{y}'\tilde{\Sigma}^{-1}\mathbf{y})\right)$	$T\Sigma - \tilde{\Sigma}^{-1} \succeq 0$
VG	$\frac{\Gamma(\frac{\tilde{\nu}+d}{2})}{\Gamma(\frac{\tilde{\nu}}{2})\tilde{\nu}^{\frac{d}{2}}\pi^{\frac{d}{2}}\sqrt{\det(\tilde{\Sigma})}} \left(1 + \frac{1}{\tilde{\nu}}(\mathbf{y}'\tilde{\Sigma}\mathbf{y})\right)^{-\frac{\tilde{\nu}+d}{2}}$	$\tilde{\nu} = \frac{2T}{\nu} - d$ , and $\Sigma - \tilde{\Sigma}^{-1} \succeq 0$ or $\tilde{\nu} \leq \frac{2T}{\nu} - d$ , and $\tilde{\Sigma} = \Sigma^{-1}$ .
NIG	$(2\pi)^{-\frac{d}{2}} (\det(\tilde{\Sigma}))^{-\frac{1}{2}} \left(\frac{\mathbf{y}'\tilde{\Sigma}^{-1}\mathbf{y}}{2}\right)^{\frac{\nu}{2}} K_{\nu}\left(\sqrt{2\mathbf{y}'\tilde{\Sigma}^{-1}\mathbf{y}}\right)$	$\delta^2 T^2 \Delta - 2\tilde{\Sigma}^{-1} \succeq 0$

### 3.2.1 Domain transformation for the GBM model

**Case of independent assets:** To simplify the preliminary analysis, we considered the case in which the stock price processes are independent. Consequently, the characteristic function of the pricing model can be written as the product of univariate characteristic functions; hence,

$$\phi_{\mathbf{X}_T}^{GBM}(\mathbf{z}) = \prod_{j=1}^d \phi_{X_T^j}^{GBM}(z_j), \mathbf{z} \in \mathbb{C}^d, \Im[\mathbf{z}] \in \delta_X^{GBM}$$

where

$$\phi_{X_T^j}^{GBM}(z_j) := \exp\left(rT - i\frac{\sigma_j^2 T}{2}z_j - \frac{\sigma_j^2 T}{2}z_j^2\right), z_j \in \mathbb{C}, \Im[z_j] \in \delta_X^{GBM}$$

Because  $\phi_{X_T^j}^{GBM}(z_j)$  is a Gaussian function, it is natural to propose that the domain transformation density is also Gaussian, in the form of  $\psi^{nor}(\mathbf{y}) = \prod_{j=1}^d \psi_j^{nor}(y_j)$ , where

$$\psi_j^{nor}(y_j) := \frac{\exp(-\frac{y_j^2}{2\tilde{\sigma}_j^2})}{\sqrt{2\tilde{\sigma}_j^2}}, \quad y_j \in \mathbb{R}, \tilde{\sigma}_j > 0,$$

and applying the change of variable (3.1), the transformed integrand is

$$\tilde{g}(\mathbf{u}) := (2\pi)^{-d} e^{-rT} e^{-\mathbf{R}'\mathbf{X}_0} \Re \left[ e^{i(\Psi_{nor}^{-1}(\mathbf{u}))'\mathbf{X}_0} \hat{P}(\Psi_{nor}^{-1}(\mathbf{u}) + i\mathbf{R}) \prod_{j=1}^d \frac{\phi_{X_T^j}^{GBM}(\Psi_{nor}^{-1}(u_j) + iR_j)}{\psi_j^{nor}(\Psi_{nor}^{-1}(u_j))} \right] \mathbf{u} \in [0, 1], \mathbf{R} \in \delta_V^{GBM}. \quad (3.5)$$

After specifying the functional form of  $\psi_j^{nor}(y_j)$ , the aim is to determine an appropriate choice of the parameters  $\{\tilde{\sigma}_j\}_{j=1}^d$ . The function  $r_j^{GBM}(\cdot)$  is defined as the ratio of the characteristic function of the variable  $X_T^j$  and the artificially introduced density  $\psi_j^{nor}(\cdot)$ :

$$r_j^{GBM}(u_j) := \frac{\phi_{X_T^j}^{GBM}(\Psi_{nor}^{-1}(u_j) + iR_j)}{\psi_j^{nor}(\Psi_{nor}^{-1}(u_j))}, u_j \in [0, 1], \mathbf{R} \in \delta_V^{GBM}.$$

The parameters  $\{\tilde{\sigma}_j\}_{j=1}^d$  should be set to control the growth of the function  $r_j^{GBM}(\cdot)$  near the boundary of  $[0, 1]$  as follows:

$$\lim_{u_j \rightarrow 0} |r_j^{GBM}(u_j)| < \infty, \forall j \in \mathbb{I}_d \iff \lim_{u_j \rightarrow 0} |\tilde{g}(\mathbf{u})| < \infty, \forall j \in \mathbb{I}_d.$$

By symmetry of the integrand  $g(\cdot)$  and the proposal density  $\psi^{nor}(\cdot)$  around the origin, it is sufficient to control the behavior of the transformed integrand as  $u_j \rightarrow 0$  to ensure that it is also controlled at all  $2^d$  corners of  $[0, 1]^d$ . Moreover, we set  $\mathbf{R} \in \delta_P$  (see Section 2); thus,  $e^{-\langle \mathbf{R}, \cdot \rangle} P(\cdot) \in L^1(\mathbb{R}^d) \Rightarrow \widehat{P}(\cdot + i\mathbf{R})$  is bounded because  $\|\widehat{P}(\cdot + i\mathbf{R})\|_{L^\infty(\mathbb{R}^d)} \leq \|e^{-\langle \mathbf{R}, \cdot \rangle} P(\cdot)\|_{L^1(\mathbb{R}^d)}$ , which is a property of Fourier transforms. Consequently, the entire transformed integrand is bounded near the boundary.

To determine the appropriate range of parameters  $\{\tilde{\sigma}_j\}_{j=1}^d$ , we replaced the characteristic function and proposed density with explicit expressions. Thus,  $r_j^{GBM}(\cdot)$  can be written as follows:

$$\begin{aligned} r_j^{GBM}(u_j) &= \exp\left(rT - \frac{iT\sigma_j^2}{2}(\Psi_{nor}^{-1}(u_j) + iR_j) - \frac{T\sigma_j^2}{2}(\Psi_{nor}^{-1}(u_j) + iR_j)^2\right) \\ &\quad \times \sqrt{2\pi\tilde{\sigma}_j^2} \exp\left(\frac{(\Psi_{nor}^{-1}(u_j))^2}{2\tilde{\sigma}_j^2}\right) \\ &= \underbrace{\tilde{\sigma}_j \exp\left(-(\Psi_{nor}^{-1}(u_j))^2 \left(\frac{T\sigma_j^2}{2} - \frac{1}{2\tilde{\sigma}_j^2}\right)\right)}_{:=h_1^{GBM}(u_j)} \\ &\quad \times \underbrace{\sqrt{2\pi} \exp\left(-i\Psi_{nor}^{-1}(u_j) \left(\frac{T\sigma_j^2}{2} - T\sigma_j^2 R_j\right) + rT - \frac{TR_j\sigma_j^2}{2} + \frac{TR_j^2\sigma_j^2}{2}\right)}_{:=h_2^{GBM}(u_j)}, \end{aligned}$$

where the function  $h_2^{GBM}(u_j)$  is bounded  $\forall u_j \in [0, 1]$ , and the function  $h_1^{GBM}(u_j)$  determines the growth of the integrand at the boundary of  $[0, 1]$ . Depending on the values of  $\{\tilde{\sigma}_j\}_{j=1}^d$ , we enumerate three possible cases

$$(3.6) \quad \lim_{u_j \rightarrow 0} h_1^{GBM}(u_j) = \begin{cases} +\infty & \text{if } \tilde{\sigma}_j < \frac{1}{\sqrt{T}\sigma_j} \quad (i), \\ \tilde{\sigma}_j < \infty & \text{if } \tilde{\sigma}_j = \frac{1}{\sqrt{T}\sigma_j} \quad (ii), \\ 0 & \text{if } \tilde{\sigma}_j > \frac{1}{\sqrt{T}\sigma_j} \quad (iii), \end{cases}$$

To summarize, a suitable choice for  $\tilde{\sigma}_j$  is  $\tilde{\sigma}_j = \bar{\sigma}_j + \epsilon_j$ , where  $\bar{\sigma}_j = \frac{1}{\sqrt{T}\sigma_j}$  defines the critical value, and  $\epsilon_j \geq 0$ . However, different values of  $\tilde{\sigma}_j$  satisfying (ii) and (iii) may lead to differing error rates of the RQMC method, as demonstrated in Section 4. Although a higher value for  $\epsilon_j$  accelerates the integrand decay, selecting an arbitrarily large  $\epsilon_j$  is not advisable because it amplifies the integrand peak around the origin and augments the magnitude of the mixed first partial derivatives of the integrand. These factors substantially influence the performance of RQMC, as illustrated in Section 4. Moreover, in Case (ii) in (3.6), the dominant term in the characteristic function vanishes, and the integrand decays at the speed of the payoff transform.

The previous derivation of the rule for the domain transformation relies on the assumption of the independence of assets. In this simplified framework, the performance of RQMC is classically

studied; however, in practical applications, the variables may be correlated. Figure 3.2 demonstrates that, when the assets are correlated, the proposed rule must be generalized to account for the correlation parameters; otherwise, the boundary growth conditions are violated, and the performance of RQMC significantly deteriorates. In the uncorrelated case, the rate of convergence of  $\mathcal{O}(N^{-1.48+\epsilon})$  is achieved. In contrast, in the positively correlated case,  $\rho = 0.7$ , the rate of RQMC is substantially smaller,  $\mathcal{O}(N^{-0.69+\epsilon})$ , and the size of the implied constant is much larger than in the uncorrelated case. To overcome this problem, in the second part of this section, we derive a domain transformation in the general case of dependent assets. Figure 3.3 illustrates that the optimal rate of RQMC is retained in the correlated setting.

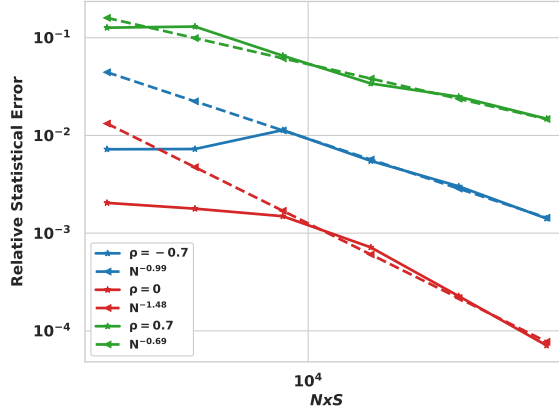


Figure 3.2: Effect of the correlation parameter,  $\rho$ , on the convergence of RQMC for a two-dimensional call on the minimum option under the GBM model with  $S_0^j = 100$ ,  $K = 100$ ,  $r = 0$ ,  $T = 1$ ,  $\sigma_j = 0.2$ ,  $j = 1, 2$ , and  $\mathbf{C} = \begin{bmatrix} 1 & \rho \\ \rho & 1 \end{bmatrix}$ . For the domain transformation,  $\tilde{\sigma}_j = \frac{1}{\sqrt{T}\sigma_j} = 5$ , where  $j = 1, 2$ .  $N$ : number of QMC points;  $S = 32$ : number of digital shifts.

**Case of dependent assets:** For dependent stocks, the joint characteristic function cannot be decomposed into the product of univariate characteristic functions, and

$$(3.7) \quad \phi_{\mathbf{X}_T}^{GBM}(\mathbf{z}) := \exp\left(\mathbf{i}\mathbf{z}'\left(\mathbf{r} - \frac{1}{2}\text{diag}(\boldsymbol{\Sigma})\right)T - \frac{T}{2}\mathbf{z}'\boldsymbol{\Sigma}\mathbf{z}\right), \quad \mathbf{z} \in \mathbb{C}^d, \Im[\mathbf{z}] \in \delta_X^{VG}.$$

Consequently, we select the proposal density  $\psi^{nor}(\cdot)$  corresponding to the multivariate normal PDF, given by

$$\psi^{nor}(\mathbf{y}) = (2\pi)^{-\frac{d}{2}}(\det(\tilde{\boldsymbol{\Sigma}}))^{-\frac{1}{2}} \exp\left(-\frac{1}{2}(\mathbf{y}'\tilde{\boldsymbol{\Sigma}}^{-1}\mathbf{y})\right), \quad \mathbf{y} \in \mathbb{R}^d, \tilde{\boldsymbol{\Sigma}} \succeq 0$$

where the matrix  $\tilde{\boldsymbol{\Sigma}}$  may have nonzero off-diagonal components. In this case, the singularity of the integrand is controlled by the function,  $r^{GBM}(\mathbf{u})$ , defined as

$$r^{GBM}(\mathbf{u}) := \frac{\phi_{\mathbf{X}_T}(\Psi_{nor}^{-1}(\mathbf{u}) + \mathbf{i}\mathbf{R})}{\psi^{nor}(\Psi_{nor}^{-1}(\mathbf{u}))}, \quad \mathbf{u} \in [0, 1]^d, \mathbf{R} \in \delta_V^{VG}.$$

By substituting in the explicit expressions of the characteristic function and proposal density, we obtain the following expression for  $r^{GBM}(\mathbf{u})$ :  $r^{GBM}(\mathbf{u})$ ,

$$(3.8) \quad r^{GBM}(\mathbf{u}) = \underbrace{(\det(\tilde{\Sigma}))^{\frac{1}{2}} \exp\left(-\frac{1}{2}(\Psi_{nor}^{-1}(\mathbf{u}))' (T\Sigma - \tilde{\Sigma}^{-1}) (\Psi_{nor}^{-1}(\mathbf{u}))\right)}_{:=h_1^{GBM}(\mathbf{u})} \times \underbrace{(2\pi)^{\frac{d}{2}} \exp\left(i(\Psi_{nor}^{-1}(\mathbf{u}) + i\mathbf{R})' \left(\mathbf{r} - \frac{1}{2} \text{diag}(\Sigma)\right) T + \frac{T}{2} \mathbf{R}' \Sigma \mathbf{R}\right)}_{:=h_2^{GBM}(\mathbf{u})}.$$

From (3.8), the function  $h_2^{GBM}(\mathbf{u})$  is bounded for  $\mathbf{u} \in [0, 1]^d$ ; hence, the part controlling the boundary growth of the integrand is given by  $h_1^{GBM}(\mathbf{u})$ . Similarly to (3.6), we enumerate three possible limits, depending on the choice of  $\tilde{\Sigma}$ :

$$(3.9) \quad \lim_{u_j \rightarrow 0} h_1^{GBM}(\mathbf{u}) = \begin{cases} +\infty & \text{if } \Sigma - \frac{1}{T} \tilde{\Sigma}^{-1} \prec 0 \text{ (i),} \\ (\det(\tilde{\Sigma}))^{\frac{1}{2}} < \infty & \text{if } \tilde{\Sigma} = \frac{1}{T} \Sigma^{-1} \text{ (ii),} \\ 0 & \text{if } \Sigma - \frac{1}{T} \tilde{\Sigma}^{-1} \succ 0 \text{ (iii).} \end{cases}$$

From (3.9), an appropriate choice of the matrix  $\tilde{\Sigma}$  satisfies either Condition (ii) or (iii). However, Condition (iii) does not result in a unique choice of the matrix  $\tilde{\Sigma}$ . The transformed integrand is multiplied by the factor  $(\det(\tilde{\Sigma}))^{\frac{1}{2}}$ ; thus, the aim is to select a matrix  $\tilde{\Sigma}$  to satisfy Condition (iii), with the minimum possible determinant to avoid high peaks of the integrand around the origin, which was motivated by previous findings (see [9]). Optimally, the choice of  $\tilde{\Sigma}$  is given by the following constrained optimization problem:

$$(3.10) \quad \begin{aligned} \tilde{\Sigma}^* &= \arg \min_{\tilde{\Sigma}} \det(\tilde{\Sigma}) \\ \text{s.t. } &\Sigma - \frac{1}{T} \tilde{\Sigma}^{-1} \succeq 0 \end{aligned}$$

Instead, we propose the following construction of the matrix  $\tilde{\Sigma}$ . The matrix  $\Sigma$  is real symmetric; thus, by the spectral theorem, it has an eigenvalue decomposition (EVD) (i.e.,  $\Sigma = \mathbf{P} \mathbf{D} \mathbf{P}^{-1}$ , with  $\mathbf{D} = \text{diag}(\lambda_1, \dots, \lambda_d)$  and  $\lambda_j > 0, j = 1, \dots, d$ ) because  $\tilde{\Sigma} \succ 0$ . To simplify the problem in (3.10), we selected the matrix  $\tilde{\Sigma}$  to be in the form of  $\tilde{\Sigma} := \mathbf{P} \tilde{\mathbf{D}} \mathbf{P}^{-1}$ , where  $\tilde{\mathbf{D}} = \text{diag}(\tilde{\lambda}_1, \dots, \tilde{\lambda}_d)$ . In this case, we can express the constraint in (3.10) as follows:

$$\mathbf{P} \left( \mathbf{D} - \frac{1}{T} \tilde{\mathbf{D}}^{-1} \right) \mathbf{P}^{-1} \succeq 0 \iff \tilde{\lambda}_j \geq \frac{1}{\lambda_j T}, j \in \mathbb{I}_d$$

Hence, a suboptimal choice for  $\tilde{\Sigma}$  is  $\tilde{\Sigma} = \mathbf{P} \text{diag}(\frac{1}{\lambda_1 T}, \dots, \frac{1}{\lambda_d T}) \mathbf{P}^{-1} = \frac{1}{T} \Sigma^{-1}$ , which is the choice adopted in this work.

Another challenge is the numerical evaluation of  $\Psi_{nor}^{-1}(\mathbf{u}; \tilde{\Sigma})$ , for which no closed-form expression or sufficiently fast approximation exists. To circumvent this problem, we expressed the multivariate normal RV with a zero mean and covariance matrix  $\tilde{\Sigma}$ ,  $\mathbf{X} \sim \mathcal{N}_d(\mathbf{0}, \tilde{\Sigma})$ , as  $\mathbf{X} = \tilde{\mathbf{L}} \mathbf{Z}$ , where  $\tilde{\mathbf{L}} \tilde{\mathbf{L}}' = \tilde{\Sigma}$  is computed via the Cholesky decomposition of  $\tilde{\Sigma}$  or  $\tilde{\mathbf{L}} = \mathbf{P} \mathbf{D}^{\frac{1}{2}}$ . In addition,  $\tilde{\Sigma} = \mathbf{P} \mathbf{D} \mathbf{P}^{-1}$  is the

EVD of the matrix  $\tilde{\Sigma}$ , and  $\mathbf{Z} \sim \mathcal{N}_d(\mathbf{0}, \mathbf{I}_d)$ . Based on this representation, we obtained the following relation:  $\Psi_{nor}^{-1}(\mathbf{u}; \tilde{\Sigma}) = \tilde{\mathbf{L}}\Psi_{nor}^{-1}(\mathbf{u}; \mathbf{I}_d)$ , where  $\Psi_{nor}^{-1}(\mathbf{u}; \mathbf{I}_d)$  can be computed elementwise using the univariate ICDF. In conclusion, the option price can be obtained by approximating the following integral using RQMC:

$$\int_{\mathbb{R}^d} g(\mathbf{y})d\mathbf{y} = \int_{[0,1]^d} \frac{g\left(\tilde{\mathbf{L}}\Psi_{nor}^{-1}(\mathbf{u}; \mathbf{I}_d)\right)}{\psi^{nor}\left(\tilde{\mathbf{L}}\Psi_{nor}^{-1}(\mathbf{u}; \mathbf{I}_d)\right)}d\mathbf{u}.$$

Figure 3.3 reveals the importance of using the general rule for the domain transformation (i.e.,  $\tilde{\Sigma} = \frac{1}{T}\Sigma$ ) compared to the rule  $\tilde{\sigma}_j = \frac{1}{\sqrt{T}\sigma_j}, j = 1, \dots, d$ , where assets are correlated. The former rule retains the optimal convergence rate of RQMC.

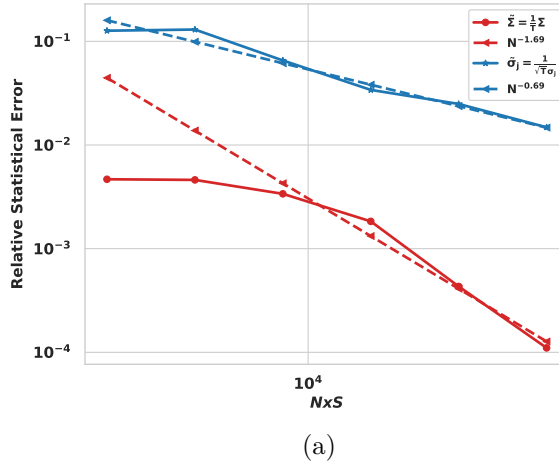


Figure 3.3: Convergence of the RQMC error for various domain transformations in the case of a two-dimensional call on the minimum option under the GBM model with  $S_0^j = 100$ ,  $K = 100$ ,  $r = 0$ ,  $T = 1$ ,  $\sigma_j = 0.2$ ,  $j = 1, 2$ , and  $\mathbf{C} = \begin{bmatrix} 1 & 0.7 \\ 0.7 & 1 \end{bmatrix}$ .  $N$ : number of QMC points;  $S = 32$ : number of digital shifts.

**Remark 3.1.** Alternative approaches to deal with the multivariate ICDF can rely on the Rosenblatt transformation [55], Nataf transformation [39] or the copula theory [48]. Investigating the efficiency of these alternatives is left for future work.

### 3.2.2 Domain transformation for the VG model

In this section we follow the same steps as in Section 3.2.1 to obtain an appropriate domain transformation for the VG model.

**Case of independent assets** This section follows the same steps as in Section 3.2.1 to obtain an appropriate domain transformation for the VG model.

**Case of independent assets:** We considered the case in which the underlying assets are independent; hence, the multivariate characteristic function can be factored into the product of the univariate characteristic functions, leading to the following relation:

$$\phi_{\mathbf{X}_T}^{VG}(\mathbf{z}) = \prod_{j=1}^d \phi_{X_T}^{VG}(z_j), \mathbf{z} \in \mathbb{C}^d, \Im[\mathbf{z}] \in \delta_X^{VG},$$

where

$$\phi_{X_T}^{VG}(z_j) = \exp(iT(r + \mu_{VG,j})z_j) \left(1 - i\nu\theta_j z_j + \frac{\nu\sigma_j^2}{2} z_j^2\right)^{-T/\nu}, z_j \in \mathbb{C}, \Im[z_j] \in \delta_X^{VG}.$$

As  $\phi_{X_T}^{VG}(z_j)$  is a rational functional, the proposal density  $\psi(\cdot)$  may also be rational. A suitable candidate density with this form is the generalized Student's  $t$ -distribution,  $\psi^{stu}(\cdot)$ . This density is written as  $\psi^{stu}(\mathbf{y}) = \prod_{j=1}^d \psi_j^{stu}(y_j)$ , where

$$\psi_j^{stu}(y_j) := \frac{\Gamma(\frac{\tilde{\nu}+1}{2})}{\sqrt{\tilde{\nu}\pi\tilde{\sigma}_j}\Gamma(\frac{\tilde{\nu}}{2})} \left(1 + \frac{y_j^2}{\tilde{\nu}\tilde{\sigma}_j^2}\right)^{-(\tilde{\nu}+1)/2}, y_j \in \mathbb{R}, \tilde{\sigma}_j > 0, \tilde{\nu} > 0,$$

Other related studies [37, 50] have typically considered the standard Student's  $t$ -distribution and not the generalized distribution. Section 4 reveals the advantage of including the scaling parameters  $\{\tilde{\sigma}_j\}_{j=1}^d$  and their effects on the convergence of RQMC. After specifying the functional form of  $\psi_j^{stu}(y_j)$ , the aim is to determine an appropriate range for the parameter  $\tilde{\nu}$ , where  $\{\tilde{\sigma}_j\}_{j=1}^d$ . We first defined the function  $r_j^{VG}(\cdot)$  as the ratio of the characteristic function of the variable  $X_T^j$  and the proposed density  $\psi_j^{stu}(\cdot)$ :

$$r_j^{VG}(u_j) := \frac{\phi_{X_T}^{VG}(\Psi_{stu}^{-1}(u_j) + iR_j)}{\psi_j^{stu}(\Psi_{stu}^{-1}(u_j))}, u_j \in [0, 1], \mathbf{R} \in \delta_V^{VG}.$$

To determine the parameters, we replaced the characteristic function and proposed density with their explicit expressions to obtain the following:

$$(3.11) \quad r_j^{VG}(u_j) := \underbrace{\sqrt{\tilde{\nu}\tilde{\sigma}_j} \times \frac{\left[ (\Psi_{stu}^{-1}(u_j))^2 \left( \frac{\nu\sigma_j^2}{2} + i\frac{\nu\sigma_j^2 R_j - \nu\theta_j}{\Psi_{stu}^{-1}(u_j)} + \frac{1 + \nu\theta_j R_j - \frac{\nu\sigma_j^2 R_j^2}{2}}{(\Psi_{stu}^{-1}(u_j))^2} \right) \right]^{-\frac{T}{\nu}}}{\left[ 1 + \frac{(\Psi_{stu}^{-1}(u_j))^2}{\tilde{\nu}\tilde{\sigma}_j^2} \right]^{-\frac{\tilde{\nu}+1}{2}}}}_{:=h_1^{VG}(u_j)} \times \underbrace{\frac{\sqrt{\pi}\Gamma(\frac{\tilde{\nu}}{2})}{\Gamma(\frac{\tilde{\nu}+1}{2})} \times \exp(iT(r + \mu_{VG,j})(\Psi_{stu}^{-1}(u_j) + iR_j))}_{:=h_2^{VG}(u_j)}.$$

The function  $h_2^{VG}(u_j)$  is bounded  $\forall u_j \in [0, 1]$ , and the function  $h_1^{VG}(u_j)$  controls the growth of the integrand at the boundary of  $[0, 1]$ , depending on the values of  $\tilde{\nu}$ . We are interested in the

asymptotic behavior of  $h_1^{VG}(u_j)$  as  $u_j \rightarrow 0 \iff \Psi^{-1}(u_j) \rightarrow -\infty$ ; thus, we approximated  $h_1^{VG}(u_j)$  near  $u_j \rightarrow 0$  as follows:

$$(3.12) \quad h_1^{VG}(u_j) = \sqrt{\tilde{\nu}}\tilde{\sigma}_j \times \frac{\left[ (\Psi_{stu}^{-1}(u_j))^2 \left( \frac{\nu\sigma_j^2}{2} + i \frac{\nu\sigma_j^2 R_j - \nu\theta_j}{\Psi_{stu}^{-1}(u_j)} + \frac{1 + \nu\theta_j R_j - \frac{\nu\sigma_j^2 R_j^2}{2}}{(\Psi_{stu}^{-1}(u_j))^2} \right) \right]^{-\frac{T}{\nu}}}{\left[ 1 + \frac{(\Psi_{stu}^{-1}(u_j))^2}{\tilde{\nu}\tilde{\sigma}_j^2} \right]^{-\frac{\tilde{\nu}+1}{2}}}$$

$$\underset{u_j \rightarrow 0}{\sim} \sqrt{\tilde{\nu}}\tilde{\sigma}_j \frac{\left[ \frac{\nu\sigma_j^2}{2} (\Psi_{stu}^{-1}(u_j))^2 \right]^{-\frac{T}{\nu}}}{\left[ \frac{(\Psi_{stu}^{-1}(u_j))^2}{\tilde{\nu}\tilde{\sigma}_j^2} \right]^{-\frac{\tilde{\nu}+1}{2}}} := \tilde{h}_1^{VG}(u_j)$$

Given the expression of  $\tilde{h}_1^{VG}(u_j)$ , we enumerate three possible limits

$$(3.13) \quad \lim_{u_j \rightarrow 0} h_1^{VG}(u_j) = \begin{cases} +\infty & \text{if } \tilde{\nu} > \frac{2T}{\nu} - 1 \text{ (i)} \\ \sqrt{\tilde{\nu}}\tilde{\sigma}_j \left[ \frac{\nu\sigma_j^2 \tilde{\nu}\tilde{\sigma}_j^2}{2} \right]^{-\frac{T}{\nu}} < \infty & \text{if } \tilde{\nu} = \frac{2T}{\nu} - 1 \text{ (ii)} \\ 0 & \text{if } \tilde{\nu} < \frac{2T}{\nu} - 1 \text{ (iii)} \end{cases}$$

From (3.13), an appropriate choice of the parameter  $\tilde{\nu}$  satisfies either the condition in Case (ii) or (iii), where (ii) implicitly relies on the constraint  $\frac{2T}{\nu} - 1 > 0$ , which, if not satisfied, implies that the characteristic function is not integrable [32]. After specifying the value of parameter  $\tilde{\nu}$ , a candidate choice for  $\{\tilde{\sigma}_j\}_{j=1}^d$  is

$$(3.14) \quad \tilde{\sigma}_j = \left[ \frac{\nu\sigma_j^2 \tilde{\nu}}{2} \right]^{\frac{T}{\nu-2T}} (\tilde{\nu})^{\frac{\nu}{4T-2\nu}}, \quad \forall j \in \mathbb{I}_d.$$

When  $\nu = \frac{2T}{\nu} - 1$ , this choice in (3.14) implies that  $\lim_{u_j \rightarrow 0} h_1^{VG}(u_j) = 1$ . Consequently, this choice reduces the adverse effect that large values of  $\tilde{\sigma}_j$  could have on the magnitude of mixed partial derivatives of the integrand, deteriorating the efficiency of RQMC. In summary, a suitable choice for  $\tilde{\nu}, \{\tilde{\sigma}_j\}_{j=1}^d$  is  $\tilde{\nu} = \bar{\nu} + \epsilon$ , where  $\bar{\nu} = \frac{2T}{\nu} - 1$  defines the critical value and  $\epsilon \geq 0$ , setting

$$\tilde{\sigma}_j = \left[ \frac{\nu\sigma_j^2 \tilde{\nu}}{2} \right]^{\frac{T}{\nu-2T}} (\tilde{\nu})^{\frac{\nu}{4T-2\nu}}.$$

**Remark 3.2.** For options with a short maturity term, such that  $\frac{2T}{\nu} - 1 < 0$ , we must use a floor value for  $\tilde{\nu}$ ; hence, we advise setting  $\tilde{\nu} = \max(\frac{2T}{\nu} - 1, 1)$ .

**Case of dependent assets** In the general case of dependent assets, we cannot factor the joint characteristic function into the product of the marginal characteristic functions as done previously, and

$$(3.15) \quad \phi_{\mathbf{X}_T}^{VG} := \exp(\mathbf{z}'(\mathbf{r} + \boldsymbol{\mu}_{VG})T) \left( 1 - i\nu\mathbf{z}'\boldsymbol{\theta} + \frac{1}{2}\mathbf{z}'\boldsymbol{\Sigma}\mathbf{z} \right), \quad \mathbf{z} \in \mathbb{C}^d, \Im[\mathbf{z}] \in \delta_X^{VG}.$$

Hence, we selected the proposal density  $\psi^{stu}(\cdot)$  corresponding to the PDF of the multivariate generalized Student-s  $t$ -distribution, given by

$$(3.16) \quad \psi^{stu}(\mathbf{y}) = \frac{C_{\tilde{\nu}}}{\sqrt{\det(\tilde{\Sigma})}} \left( 1 + \frac{1}{\tilde{\nu}} \left( \mathbf{y}' \tilde{\Sigma}^{-1} \mathbf{y} \right) \right)^{-\frac{\tilde{\nu}+d}{2}}, \quad \mathbf{y} \in \mathbb{R}^d, \tilde{\nu} > 0, \tilde{\Sigma} \succ 0$$

where

$$(3.17) \quad C_{\tilde{\nu}} := \frac{\Gamma\left(\frac{\tilde{\nu}+d}{2}\right)}{\Gamma\left(\frac{\tilde{\nu}}{2}\right) \tilde{\nu}^{\frac{d}{2}} \pi^{\frac{d}{2}}} > 0.$$

Then, the function  $r^{VG}(\mathbf{u})$  controls the growth of the integrand near the boundary:

$$(3.18) \quad r^{VG}(\mathbf{u}) := \frac{\phi_{\mathbf{X}_T}^{VG}(\Psi^{-1}(\mathbf{u}) + \mathbf{i}\mathbf{R})}{\psi^{stu}(\Psi^{-1}(\mathbf{u}))}, \quad \mathbf{u} \in [0, 1]^d, \mathbf{R} \in \delta_V^{VG}.$$

The characteristic function can be approximated near  $u_j \rightarrow 0$  as follows,

$$(3.19) \quad \begin{aligned} \phi_{\mathbf{X}_T}^{VG}(\Psi^{-1}(\mathbf{u}) + \mathbf{i}\mathbf{R}) &= \exp(T(\mathbf{i}\Psi^{-1}(\mathbf{u}) - \mathbf{R})' \boldsymbol{\mu}_{VG}) \\ &\times \left( \frac{\nu}{2} ((\Psi^{-1}(\mathbf{u}))' \boldsymbol{\Sigma} \Psi^{-1}(\mathbf{u})) \left( 1 + 2\mathbf{i} \frac{((\Psi^{-1}(\mathbf{u}))' \boldsymbol{\Sigma} \mathbf{R})}{(\Psi^{-1}(\mathbf{u}))' \boldsymbol{\Sigma} \Psi^{-1}(\mathbf{u}))} \right. \right. \\ &\left. \left. + \frac{1 - \nu \boldsymbol{\theta}'(\mathbf{i}\Psi^{-1}(\mathbf{u}) - \mathbf{R}) - \frac{1}{2}\nu(\mathbf{R}' \boldsymbol{\Sigma} \mathbf{R})}{(\Psi^{-1}(\mathbf{u}))' \boldsymbol{\Sigma} \Psi^{-1}(\mathbf{u}))} \right) \right)^{-T/\nu} \\ &\stackrel{u_j \rightarrow 0}{\sim} \exp(T(\mathbf{i}\Psi^{-1}(\mathbf{u}) - \mathbf{R})' \boldsymbol{\mu}_{VG}) \times \left( \frac{\nu}{2} ((\Psi^{-1}(\mathbf{u}))' \boldsymbol{\Sigma} \Psi^{-1}(\mathbf{u})) \right)^{-T/\nu} \end{aligned}$$

Furthermore, the multivariate generalized Student's  $t$  density can be approximated asymptotically as  $u_j \rightarrow 0$  by

$$(3.20) \quad \psi^{stu}(\Psi^{-1}(\mathbf{u})) \stackrel{u_j \rightarrow 0}{\sim} \frac{C_{\tilde{\nu}}}{\sqrt{\det(\tilde{\Sigma})}} \left( \frac{1}{\tilde{\nu}} (\Psi^{-1}(\mathbf{u}))' \tilde{\Sigma}^{-1} \Psi^{-1}(\mathbf{u}) \right)^{-\frac{\tilde{\nu}+d}{2}}$$

By applying the asymptotic relations in (3.19) and (3.20), we approximated the function  $r^{VG}(\mathbf{u})$  as follows:

$$(3.21) \quad \begin{aligned} r^{VG}(\mathbf{u}) &\stackrel{u_j \rightarrow 0}{\sim} \underbrace{\exp(T(\mathbf{i}\Psi^{-1}(\mathbf{u}) - \mathbf{R})' \boldsymbol{\mu}_{VG}) \exp\left(-\frac{T}{\nu} \log\left(\frac{\nu}{2}\right) + \frac{\tilde{\nu}+d}{2} \log\left(\frac{1}{\tilde{\nu}}\right)\right)}_{h_2^{VG}(\mathbf{u})} \times \\ &\frac{\sqrt{\det(\tilde{\Sigma})}}{C_{\tilde{\nu}}} \underbrace{\exp\left(-\left(\frac{T}{\nu} \log((\Psi^{-1}(\mathbf{u}))' \boldsymbol{\Sigma} \Psi^{-1}(\mathbf{u})) - \frac{\tilde{\nu}+d}{2} \log((\Psi^{-1}(\mathbf{u}))' \tilde{\Sigma}^{-1} \Psi^{-1}(\mathbf{u}))\right)\right)}_{h_1^{VG}(\mathbf{u})} \end{aligned}$$

The function  $h_2^{VG}(\mathbf{u})$  remains bounded  $\forall \mathbf{u} \in [0, 1]^d$ ; hence, the function  $h_1^{VG}(\mathbf{u})$  controls the boundary growth of the integrand. In contrast to the case of GBM, the removal of the singularity

at the boundary depends on the interplay of two parameters:  $\tilde{\nu}$  and the covariance matrix  $\tilde{\Sigma}$ . By the monotonicity of  $x \mapsto \log(x)$ , selecting  $\tilde{\nu} = \frac{2T}{\nu} - d$  results in the following:

$$(3.22) \quad \log((\Psi^{-1}(\mathbf{u}))' \Sigma \Psi^{-1}(\mathbf{u})) - \log((\Psi^{-1}(\mathbf{u}))' \tilde{\Sigma}^{-1} \Psi^{-1}(\mathbf{u})) \geq 0 \iff (\Psi^{-1}(\mathbf{u}))' (\Sigma - \tilde{\Sigma}^{-1}) \Psi^{-1}(\mathbf{u}) \geq 0$$

Equation (3.22) indicates that if  $\tilde{\nu} = \frac{2T}{\nu} - d$ , then three possible cases exist:

$$(3.23) \quad \lim_{u_j \rightarrow 0} h_1^{VG}(\mathbf{u}) = \begin{cases} +\infty & \text{if } \Sigma - \tilde{\Sigma}^{-1} \prec 0 \text{ (i),} \\ \frac{\sqrt{\det(\tilde{\Sigma})}}{C_{\tilde{\nu}}} & \text{if } \tilde{\Sigma} = \Sigma^{-1} \text{ (ii),} \\ 0 & \text{if } \Sigma - \tilde{\Sigma}^{-1} \succ 0 \text{ (iii).} \end{cases}$$

From (3.23), if  $\tilde{\nu} = \frac{2T}{\nu} - d$ , an appropriate choice of  $\tilde{\Sigma}$  is one such that  $\Sigma - \tilde{\Sigma}^{-1} \succeq 0$ , but with smallest possible eigenvalues to minimize the term  $\sqrt{\det(\tilde{\Sigma})}$ . In contrast, for (3.21), setting  $\tilde{\Sigma} = \Sigma^{-1}$  provides the following three possible cases:

$$(3.24) \quad \lim_{u_j \rightarrow 0} h_1^{VG}(\mathbf{u}) = \begin{cases} +\infty & \text{if } \tilde{\nu} > \frac{2T}{\nu} - d \text{ (i),} \\ \frac{\sqrt{\det(\tilde{\Sigma})}}{C_{\tilde{\nu}}} & \text{if } \tilde{\nu} = \frac{2T}{\nu} - d \text{ (ii),} \\ 0 & \text{if } \tilde{\nu} < \frac{2T}{\nu} - d \text{ (iii).} \end{cases}$$

From (3.24), if  $\tilde{\Sigma} = \Sigma^{-1}$ , an appropriate choice of  $\tilde{\nu}$  is given by  $\tilde{\nu} = \bar{\nu} - \epsilon$ , where  $\bar{\nu} = \frac{2T}{\nu} - d$ ,  $\epsilon \geq 0$ . In this case, increasing the value of  $\epsilon$  decreases the value of  $\tilde{\nu}$ , which increases the value of  $C_{\tilde{\nu}} \propto (\tilde{\nu})^{-\frac{d}{2}}$  and reduces the constant factor multiplied by the integrand. This result indicates that, for a fixed  $\tilde{\Sigma} = \Sigma^{-1}$ , reducing the value of  $\tilde{\nu}$  may improve the performance of RQMC.

Similarly to the case of GBM, the suggested domain transformation necessitates the numerical evaluation of the ICDF of the multivariate generalized Student's  $t$ -distribution,  $\Psi^{-1}(\mathbf{u})$ . This inversion poses numerical challenges because it cannot be performed componentwise as it can in independent assets. Consequently, we adopted a similar approach to that employed for the GBM model. We represent the generalized Student's  $t$ -distribution in the multivariate normal variance mixture form and use the Cholesky or principal component factorization to eliminate the dependence structure. This representation (see Equation (B.2)) is a critical tool that avoids the computation of the ICDF, as presented in Proposition 3.3.

**Proposition 3.3.** *We let  $g(\cdot)$  denote the integrand defined in (2.2). Then, its integral over  $\mathbb{R}^d$  can be expressed using Fubini's theorem, as follows:*

$$(3.25) \quad \int_{\mathbb{R}^d} g(\mathbf{y}) d\mathbf{y} = \int_0^{+\infty} \left( \int_{[0,1]^d} \frac{g\left(\frac{\tilde{\mathbf{L}} \cdot \Psi_{nor}^{-1}(\mathbf{u}; \mathbf{I}_d)}{w}\right)}{\psi_{stu}\left(\frac{\tilde{\mathbf{L}} \cdot \Psi_{nor}^{-1}(\mathbf{u}; \mathbf{I}_d)}{w}\right)} d\mathbf{u} \right) \psi_{chi}(w) dw,$$

where  $\psi_{chi}(w) := \frac{2^{-\frac{\tilde{\nu}}{2}+1}}{\Gamma(\frac{\tilde{\nu}}{2})} w^{\tilde{\nu}-1} \exp\left(-\frac{w^2}{2}\right)$  is the PDF of the chi distribution with degrees of freedom,  $\tilde{\nu}$ , and  $\tilde{\mathbf{L}}$  is the Cholesky factor of the matrix  $\tilde{\nu} \times \tilde{\Sigma}$  in (3.16).

*Proof.* Appendix B presents the proof. □

From (3.25), the proposed transformation results in an additional integral over  $[0, +\infty)$  against the PDF of the chi-squared distribution. To compute the resulting nested integral in (3.25), we propose a hybrid approach that consists of applying the Gauss–Laguerre quadrature for the outer integral and employing RQMC for the inner integral. The proposed approximation can be written as follows:

$$(3.26) \quad \int_{\mathbb{R}^d} g(\mathbf{y}) d\mathbf{y} \approx \frac{1}{N \times S} \sum_{s=1}^S \sum_{n=1}^N \left( \sum_{m=1}^{M_{Lag}} \frac{\omega_m}{\lambda_{Lag}(y_m)} \frac{g\left(\frac{\tilde{\mathbf{L}} \cdot \Psi_{\text{nor}}^{-1}(\mathbf{u}_n^{(s)}; \mathbf{I}_d)}{y_m}\right)}{\psi_{\text{stu}}\left(\frac{\tilde{\mathbf{L}} \cdot \Psi_{\text{nor}}^{-1}(\mathbf{u}_n^{(s)}; \mathbf{I}_d)}{y_m}\right)} \right) \psi_{\text{chi}}(y_m)$$

where  $\{y_m\}_{m=1}^{M_{Lag}}$  and  $\{\omega_m\}_{m=1}^{M_{Lag}}$  denote the Gauss–Laguerre quadrature nodes and quadrature weights, respectively. In addition,  $\lambda_{Lag}(\cdot)$  represents the weight function corresponding to the Gauss–Laguerre quadrature rule (i.e.,  $\lambda_{Lag}(y_m) = \exp(-y_m)$ ).

**Remark 3.4.** In contrast to the GBM and NIG models, the characteristic function of the VG model decays polynomially, implying that, if the payoff transform also decays polynomially, the boundary growth of the integrand is no longer dominated by the ratio of the characteristic function and proposal density. Consequently, the conditions derived in (3.13), (3.23), and (3.24) are rather conservative. Even if the boundary growth conditions are not strictly satisfied, we may not observe singularity at the boundary because the decay of the payoff transform is faster than the growth of  $r^{VG}(\cdot)$ .

### 3.2.3 Domain transformation for the NIG model

**Case of independent assets** Following the same scheme as in Sections 3.2.1 and 3.2.2, we consider the setting of independent stocks; hence, we have

$$(3.27) \quad \phi_{\mathbf{X}_T}^{NIG}(\mathbf{z}) = \prod_{j=1}^d \phi_{X_T^j}^{NIG}(z_j), \mathbf{z} \in \mathbb{C}^d, \Im[\mathbf{z}] \in \delta_X^{NIG},$$

where

$$(3.28) \quad \phi_{X_T^j}^{NIG}(z_j) = \exp\left(iz_j(r + \mu_j^{NIG})T + \delta T \left(\sqrt{\alpha^2 - \beta_j^2} - \sqrt{\alpha^2 - (\beta_j + iz_j)^2}\right)\right), z_j \in \mathbb{C}.$$

As  $\phi_{X_T^j}^{NIG}(z_j)$  is a root-exponential function, the density we propose for the domain transformation is the density of the Laplace distribution, also known as the double-sided exponential distribution, given by  $\psi^{lap}(\mathbf{y}) = \prod_{j=1}^d \psi_j^{lap}(y_j)$ , where

$$(3.29) \quad \psi_j^{lap}(y_j; \tilde{\sigma}_j) = \frac{\exp(-\frac{|y_j|}{\tilde{\sigma}_j})}{2\tilde{\sigma}_j}, y_j \in \mathbb{R}, \tilde{\sigma}_j > 0.$$

Upon defining the functional form of  $\psi_j^{lap}(u_j)$ , the objective is to identify an appropriate selection for the parameters  $\{\tilde{\sigma}_j\}_{j=1}^d$ . To begin, we introduce the function  $r_j^{NIG}(\cdot)$ , representing the ratio of

the characteristic function of the NIG-distributed RV  $X_T^j$  to the density  $\psi_j^{lap}(\cdot)$ :

$$(3.30) \quad r_j^{NIG}(u_j) := \frac{\phi_{X_T^j}^{NIG}(\Psi_{lap}^{-1}(u_j) + iR_j)}{\psi_j^{lap}(\Psi_{lap}^{-1}(u_j))}, u_j \in [0, 1], \mathbf{R} \in \delta_V^{NIG}.$$

Then,  $r_j^{NIG}(u_j)$  can be expressed by inserting the explicit expressions of the characteristic function and density as follows:

$$(3.31) \quad r_j^{NIG}(u_j) = \underbrace{\tilde{\sigma}_j \exp \left( -|\Psi_{lap}^{-1}(u_j)| \left( \delta T \sqrt{1 + \frac{2i(R_j - \beta_j)}{\Psi_{lap}^{-1}(u_j)}} + \frac{(\alpha^2 - (\beta_j - R_j)^2)}{(\Psi_{lap}^{-1}(u_j))^2} - \frac{1}{\tilde{\sigma}_j} \right)}_{:=h_1^{NIG}(u_j)} \right)}_{:=h_2^{NIG}(u_j)} \times 2 \exp \left( i(\Psi_{lap}^{-1}(u_j) + iR_j)(r + \mu_j^{NIG})T + \delta T \sqrt{\alpha^2 - \beta_j^2} \right), u_j \in [0, 1].$$

In (3.31), the function  $h_2^{NIG}(u_j)$  remains bounded for  $u_j \in [0, 1]$ , and the function  $h_1^{NIG}(u_j)$  controls the boundary growth of the integrand as  $u_j \rightarrow 0 \Rightarrow |\Psi_{lap}^{-1}(u_j)| \rightarrow +\infty$ . To analyze the function  $h_1^{NIG}(u_j)$  in (3.31), we derived its limiting behavior at the boundary of  $[0, 1]$ :

$$(3.32) \quad h_1^{NIG}(u_j) = \tilde{\sigma}_j \exp \left( -|\Psi_{lap}^{-1}(u_j)| \left( \delta T \sqrt{1 + \frac{2i(R_j - \beta_j)}{\Psi_{lap}^{-1}(u_j)}} + \frac{(\alpha^2 - (\beta_j - R_j)^2)}{(\Psi_{lap}^{-1}(u_j))^2} - \frac{1}{\tilde{\sigma}_j} \right) \right) \underset{u_j \rightarrow 0}{\sim} \underbrace{\tilde{\sigma}_j \exp \left( -|\Psi_{lap}^{-1}(u_j)| \left( \delta T - \frac{1}{\tilde{\sigma}_j} \right) \right)}_{:=\tilde{h}_1^{NIG}(u_j)}.$$

Three possible limits are outlined by focusing on the behavior of the term  $\tilde{h}_1^{NIG}(u_j)$  in (3.32) as  $u_j \rightarrow 0$ :

$$(3.33) \quad \lim_{u_j \rightarrow 0} \tilde{h}_1^{NIG}(u_j) = \begin{cases} +\infty & \text{if } \tilde{\sigma}_j < \frac{1}{\delta T} \text{ (i)}, \\ \tilde{\sigma}_j & \text{if } \tilde{\sigma}_j = \frac{1}{\delta T} \text{ (ii)}, \\ 0 & \text{if } \tilde{\sigma}_j > \frac{1}{\delta T} \text{ (iii)}. \end{cases}$$

From (3.42), an appropriate choice of the parameters  $\{\tilde{\sigma}_j\}_{j=1}^d$  satisfies either the condition in (ii) or (iii) (i.e.,  $\tilde{\sigma}_j = \bar{\sigma}_j + \epsilon_j$ , where  $\bar{\sigma}_j = \frac{1}{\delta T}$  and  $\epsilon \geq 0$ ). Despite larger values of  $\epsilon_j$  resulting in a faster decay of the integrand to zero, they concurrently amplify the magnitude of the mixed first partial derivatives. Consequently, relatively large values of  $\tilde{\sigma}_j$  may degrade the performance of RQMC in high dimensions.

**Case of dependent assets:** The multivariate characteristic function of the NIG model is given by

$$(3.34) \quad \phi_{\mathbf{X}_T}^{NIG}(z) = \exp \left( i\mathbf{z}'(\mathbf{r} + \boldsymbol{\mu}_{NIG})T + \delta T \left( \sqrt{\alpha^2 - \boldsymbol{\beta}'\boldsymbol{\Delta}\boldsymbol{\beta}} - \sqrt{\alpha^2 - (\boldsymbol{\beta} + i\mathbf{z})'\boldsymbol{\Delta}(\boldsymbol{\beta} + i\mathbf{z})} \right) \right).$$

Consequently, the density that matches the functional form of the characteristic function, corresponding to the multivariate Laplace distribution, is selected

$$(3.35) \quad \psi_{lap}(\mathbf{y}) = \frac{2}{(2\pi)^{\frac{d}{2}} \sqrt{\det(\tilde{\Sigma})}} \left( \frac{\mathbf{y}' \tilde{\Sigma}^{-1} \mathbf{y}}{2} \right)^{\frac{v}{2}} K_v \left( \sqrt{2\mathbf{y}' \tilde{\Sigma}^{-1} \mathbf{y}} \right), \mathbf{y} \in \mathbb{R}^d, \tilde{\Sigma} \succeq 0,$$

where  $v = \frac{2-d}{2}$ , and  $K_v(\cdot)$  is the modified Bessel function of the third kind. To determine a rule for the choice of  $\tilde{\Sigma}$ , we analyze the tail behavior of the function  $r^{NIG}(\mathbf{u})$ :

$$(3.36) \quad r^{NIG}(\mathbf{u}) := \frac{\phi_{\mathbf{X}_T}^{NIG}(\Psi_{lap}^{-1}(\mathbf{u}) + \mathbf{iR})}{\psi_{lap}(\Psi_{lap}^{-1}(\mathbf{u}))}, \mathbf{u} \in [0, 1]^d, \mathbf{R} \in \delta_V^{NIG}.$$

We evaluated the behavior of  $r^{NIG}(\mathbf{u})$  as  $u_j \rightarrow 0, j \in \mathbb{I}_d$ , where the characteristic function can be approximated as follows:

$$(3.37) \quad \begin{aligned} \phi_{\mathbf{X}_T}^{NIG}(\mathbf{u} + \mathbf{iR}) &= \exp \left( iT(\Psi_{lap}^{-1}(\mathbf{u}))' \boldsymbol{\mu}_{NIG} - T\mathbf{R}' \boldsymbol{\mu}_{NIG} + \delta T \sqrt{\alpha^2 - \boldsymbol{\beta}' \boldsymbol{\Delta} \boldsymbol{\beta}} \right) \times \\ &\quad \exp \left( -\delta T \sqrt{\alpha^2 - (\boldsymbol{\beta} - \mathbf{R})' \boldsymbol{\Delta} (\boldsymbol{\beta} - \mathbf{R}) - 2i(\Psi_{lap}^{-1}(\mathbf{u}))' \boldsymbol{\Delta} (\boldsymbol{\beta} - \mathbf{R}) + (\Psi_{lap}^{-1}(\mathbf{u}))' \boldsymbol{\Delta} \Psi_{lap}^{-1}(\mathbf{u})} \right) \\ &= \exp \left( iT(\Psi_{lap}^{-1}(\mathbf{u}))' \boldsymbol{\mu}_{NIG} - T\mathbf{R}' \boldsymbol{\mu}_{NIG} + \delta T \sqrt{\alpha^2 - \boldsymbol{\beta}' \boldsymbol{\Delta} \boldsymbol{\beta}} \right) \times \\ &\quad \exp \left( -\delta T \sqrt{(\Psi_{lap}^{-1}(\mathbf{u}))' \boldsymbol{\Delta} \Psi_{lap}^{-1}(\mathbf{u})} \sqrt{1 - \frac{\alpha^2 - (\boldsymbol{\beta} - \mathbf{R})' \boldsymbol{\Delta} (\boldsymbol{\beta} - \mathbf{R})}{(\Psi_{lap}^{-1}(\mathbf{u}))' \boldsymbol{\Delta} \Psi_{lap}^{-1}(\mathbf{u})} - \frac{2i(\Psi_{lap}^{-1}(\mathbf{u}))' \boldsymbol{\Delta} (\boldsymbol{\beta} - \mathbf{R})}{(\Psi_{lap}^{-1}(\mathbf{u}))' \boldsymbol{\Delta} \Psi_{lap}^{-1}(\mathbf{u})}} \right) \\ &\stackrel{u_j \rightarrow 0}{\sim} \exp \left( iT(\Psi_{lap}^{-1}(\mathbf{u}))' \boldsymbol{\mu}_{NIG} - T\mathbf{R}' \boldsymbol{\mu}_{NIG} + \delta T \sqrt{\alpha^2 - \boldsymbol{\beta}' \boldsymbol{\Delta} \boldsymbol{\beta}} \right) \times \\ &\quad \exp \left( -\delta T \sqrt{(\Psi_{lap}^{-1}(\mathbf{u}))' \boldsymbol{\Delta} \Psi_{lap}^{-1}(\mathbf{u})} \right), \quad \text{as } u_j \rightarrow 0, j \in \mathbb{I}_d. \end{aligned}$$

Moreover, for large values of  $y \in \mathbb{R}$ , we have that

$$(3.38) \quad K_v(y) \stackrel{|y| \rightarrow \infty}{\sim} K_{\frac{1}{2}}(y) = \sqrt{2\pi} \frac{\exp(-y)}{\sqrt{2y}}.$$

Hence, the density of the multivariate Laplace distribution can be asymptotically approximated as

follows:

$$\begin{aligned}
\psi_{lap}(\Psi_{lap}^{-1}(\mathbf{u})) &= \frac{2}{(2\pi)^{\frac{d}{2}} \sqrt{\det(\tilde{\Sigma})}} \left( \frac{\Psi_{lap}^{-1}(\mathbf{u})' \tilde{\Sigma}^{-1} \Psi_{lap}^{-1}(\mathbf{u})}{2} \right)^{\frac{v}{2}} \\
&\quad \times K_v \left( \sqrt{2\Psi_{lap}^{-1}(\mathbf{u})' \tilde{\Sigma}^{-1} \Psi_{lap}^{-1}(\mathbf{u})} \right) \\
(3.39) \quad &\underset{u_j \rightarrow 0}{\sim} \frac{2\sqrt{2\pi}}{(2\pi)^{\frac{d}{2}} \sqrt{\det(\tilde{\Sigma})}} \left( \frac{\Psi_{lap}^{-1}(\mathbf{u})' \tilde{\Sigma}^{-1} \Psi_{lap}^{-1}(\mathbf{u})}{2} \right)^{\frac{v}{2}} \\
&\quad \times \frac{\exp \left( -\sqrt{2\Psi_{lap}^{-1}(\mathbf{u})' \tilde{\Sigma}^{-1} \Psi_{lap}^{-1}(\mathbf{u})} \right)}{\sqrt{2\sqrt{2\Psi_{lap}^{-1}(\mathbf{u})' \tilde{\Sigma}^{-1} \Psi_{lap}^{-1}(\mathbf{u})}}}.
\end{aligned}$$

With both the asymptotic approximations presented in (3.37) and (3.39), the boundary growth of  $r^{NIG}(\mathbf{u})$  is controlled by the following term:

$$(3.40) \quad h_1^{NIG}(\mathbf{u}) := \sqrt{\det(\tilde{\Sigma})} \exp \left( -(\delta T \sqrt{(\Psi_{lap}^{-1}(\mathbf{u})' \mathbf{\Delta} \Psi_{lap}^{-1}(\mathbf{u}) - \sqrt{2(\Psi_{lap}^{-1}(\mathbf{u})' \tilde{\Sigma}^{-1} \Psi_{lap}^{-1}(\mathbf{u}))})} \right)$$

In general, the function  $x \mapsto \sqrt{x}$  is monotonic; thus,

$$(3.41) \quad \sqrt{\delta^2 T^2 (\Psi_{lap}^{-1}(\mathbf{u})' \mathbf{\Delta} \Psi_{lap}^{-1}(\mathbf{u}) - \sqrt{2(\Psi_{lap}^{-1}(\mathbf{u})' \tilde{\Sigma}^{-1} \Psi_{lap}^{-1}(\mathbf{u}))})} \geq 0 \iff (\Psi_{lap}^{-1}(\mathbf{u})' (\delta^2 T^2 \mathbf{\Delta} - 2\tilde{\Sigma}^{-1}) \Psi_{lap}^{-1}(\mathbf{u})) \geq 0.$$

Therefore, three possible cases exist:

$$(3.42) \quad \lim_{u_j \rightarrow 0} h_1^{NIG}(\mathbf{u}) = \begin{cases} +\infty & \text{if } \delta^2 T^2 \mathbf{\Delta} - 2\tilde{\Sigma}^{-1} \prec 0 \text{ (i),} \\ \sqrt{\det(\tilde{\Sigma})} & \text{if } \tilde{\Sigma} = \frac{2}{\delta^2 T^2} \mathbf{\Delta}^{-1} \text{ (ii),} \\ 0 & \text{if } \delta^2 T^2 \mathbf{\Delta} - 2\tilde{\Sigma}^{-1} \succ 0 \text{ (iii).} \end{cases}$$

From (3.42), a sufficient condition to eliminate the singularity at the boundary is to set  $\tilde{\Sigma}$  such that the matrix  $\delta^2 T^2 \mathbf{\Delta} - 2\tilde{\Sigma}^{-1} \succeq 0$ . The problem of finding such a matrix does not have a unique solution; hence, we propose a candidate construction similar to that in Section 3.2.1. The matrix  $\mathbf{\Delta}$  is a real symmetric matrix; thus, via the spectral theorem, it has a principal value factorization (i.e.,  $\mathbf{\Delta} = \mathbf{P} \mathbf{D} \mathbf{P}^{-1}$ ), where  $\mathbf{D} = \text{diag}(\lambda_1, \dots, \lambda_d)$  with  $\lambda_j > 0, j = 1, \dots, d$ , because  $\mathbf{\Delta}$  is PD. Therefore, we propose the construction  $\tilde{\Sigma} := \mathbf{P} \tilde{\mathbf{D}} \mathbf{P}^{-1}$ , where  $\tilde{\mathbf{D}} = \text{diag}(\tilde{\lambda}_1, \dots, \tilde{\lambda}_d)$  such that  $\delta^2 T^2 \mathbf{\Delta} - 2\tilde{\Sigma}^{-1} \succeq 0$ . This condition can be rewritten as follows:

$$(3.43) \quad \mathbf{P}(\delta^2 T^2 \mathbf{D} - 2\tilde{\mathbf{D}}^{-1}) \mathbf{P}^{-1} \succeq 0 \iff \tilde{\lambda}_j \geq \frac{2}{\lambda_j \delta^2 T^2}, j \in \mathbb{I}_d.$$

Furthermore, the integrand is proportional to  $\det(\tilde{\Sigma}) = \prod_{j=1}^d \tilde{\lambda}_j$ ; therefore, the aim is to select the matrix with a minimal determinant that satisfies the inequality in (3.43). Consequently, we constructed the matrix  $\tilde{\Sigma}$  by setting  $\tilde{\Sigma} = \mathbf{P} \text{diag}(\frac{2}{\lambda_1 \delta^2 T^2}, \dots, \frac{2}{\lambda_d \delta^2 T^2}) \mathbf{P}^{-1} = \frac{2}{\delta^2 T^2} \mathbf{\Delta}^{-1}$ .

Moreover, similarly to the case for VG, the ICDF,  $\Psi_{lap}^{-1}(\mathbf{u})$ , does not have a closed-form expression or efficient numerical approximation. To overcome this challenge, we represent the multivariate Laplace distribution as a mixture of normal distributions, as stated in Theorem 6.3.1 in [34], and derive an alternative integral representation of (2.1) that avoids the computation of  $\Psi_{lap}^{-1}(\cdot)$ .

**Proposition 3.5.** *We let  $g(\cdot)$  denote the integrand defined in (2.2), then its integral over  $\mathbb{R}^d$  can be expressed using Fubini's theorem, as follows:*

$$(3.44) \quad \int_{\mathbb{R}^d} g(\mathbf{y}) d\mathbf{y} = \int_0^{+\infty} \left( \int_{[0,1]^d} \frac{g\left(w\tilde{\mathbf{L}} \cdot \Psi_{nor}^{-1}(\mathbf{u}; \mathbf{I}_d)\right)}{\psi_{lap}\left(w\tilde{\mathbf{L}} \cdot \Psi_{nor}^{-1}(\mathbf{u}; \mathbf{I}_d)\right)} d\mathbf{u} \right) \psi_{ray}(w) dw,$$

where  $\psi_{ray}(w) = 2w \exp(-w^2)$  denotes the PDF of the Rayleigh distribution with scale  $\frac{1}{\sqrt{2}}$ , and  $\tilde{\mathbf{L}}$  is the Cholesky factor of the matrix  $\tilde{\Sigma}$  in (3.35).

*Proof.* Appendix C presents the proof. □

In (3.44), the integral is approximated numerically using a hybrid scheme with the Gauss–Laguerre quadrature for the outer integral and the RQMC quadrature for the inner integral, yielding the following estimator:

$$(3.45) \quad \int_{\mathbb{R}^d} g(\mathbf{y}) d\mathbf{y} \approx \frac{1}{N \times S} \sum_{s=1}^S \sum_{n=1}^N \left( \sum_{m=1}^{M_{Lag}} \frac{\omega_m}{\lambda_{Lag}(y_m)} \frac{g\left(w\tilde{\mathbf{L}} \cdot \Psi_{nor}^{-1}(\mathbf{u}_n^{(s)}; \mathbf{I}_d)\right)}{\psi_{lap}\left(w\tilde{\mathbf{L}} \cdot \Psi_{nor}^{-1}(\mathbf{u}_n^{(s)}; \mathbf{I}_d)\right)} \psi_{\sqrt{W}}(y_m) \right),$$

where  $\{y_m\}_{m=1}^{M_{Lag}}$  and  $\{\omega_m\}_{m=1}^{M_{Lag}}$  are the Gauss–Laguerre quadrature nodes and quadrature weights, respectively. In addition,  $\lambda_{Lag}(\cdot)$  represents the weight function corresponding to the Gauss–Laguerre quadrature rule (i.e.,  $\lambda_{Lag}(y_m) = \exp(-y_m)$ ).

**Remark 3.6** (Choice of the proposal distribution). In principle, we could employ the multivariate Student's  $t$  PDF in the transformation for all three considered pricing models (GBM, VG, and NIG) because, for GBM and NIG, the decay of the characteristic function is exponential, which is faster than the power-law decay of the density of the Student's  $t$ -distribution. However, this approach would have two consequences. It would alter the original integrand features and be more challenging to motivate a theoretical choice for the parameters of the proposal density.

**Remark 3.7** (Damping parameters). The value of the damping parameters is independent of the domain transformation; thus, the rule proposed in [9] remains the same in this work. The independence comes from using the damping parameters that minimize the peak of the integrand at the origin, corresponding to  $\Psi^{-1}(\mathbf{u}) = \mathbf{0}$  for the transformed integrand. Hence, the original integrand is divided by  $\psi(\mathbf{0})$ , a constant term independent of  $\mathbf{R}$ .

**Remark 3.8** (On the choice of the optimizer). For high-dimensional problems  $d > 10$ , some optimizers, such as L-BFGS-B [64], may not converge to the optimal solution. However, the trust-region method (see [12]) was empirically observed to be more robust in high dimensions.

## 4 Numerical Experiments and Results

This section presents the results of numerical experiments conducted for pricing multiasset European basket put and call on minimum (call on min) options with the respective payoffs:

$$(i) P(\mathbf{X}_T; K) = \max \left( K - \frac{1}{d} \sum_{i=1}^d e^{X_T^i}, 0 \right); \quad (ii) P(\mathbf{X}_T; K) = \max \left( \min \left( e^{X_T^1}, \dots, e^{X_T^d} \right) - K, 0 \right).$$

Table 4.1 presents the scaled version of these payoffs and their Fourier transforms. These payoff functions adhere to the assumption outlined in 2.2. Further details on their derivation are provided in [17, 29, 30]

Payoff	$P(\mathbf{X}_T)$	$\hat{P}(z)$	$\delta_P$
Basket put	$\max \left( 1 - \sum_{i=1}^d e^{X_T^i}, 0 \right)$	$\frac{\prod_{j=1}^d \Gamma(-iz_j)}{\Gamma(-i \sum_{j=1}^d z_j + 2)}$	$\{\Im[z_j] > 0\}$
Call on min	$\max \left( \min \left( e^{X_T^1}, \dots, e^{X_T^d} \right) - 1, 0 \right)$	$\frac{1}{(i(\sum_{j=1}^d z_j) - 1) \prod_{j=1}^d (iz_j)}$	$\{\Im[z_j] < 0, \sum_{j=1}^d \Im[z_j] < -1\}$

Table 4.1: Payoff functions (scaled),  $P(\mathbf{X}_T)$ , their extended Fourier transform,  $\hat{P}(z)$ , and the corresponding domain of analyticity,  $\delta_P$ .  $\Gamma(z) = \int_0^{+\infty} e^{-t} t^{z-1} dt$  denotes the complex Gamma function defined for  $z \in \mathbb{C}$  with  $\Re[z] > 0$ .

We tested the performance of RQMC with the appropriate domain transformation (see Section 3) for the GBM, VG, and NIG models with various parameter constellations and dimensions  $d \in \{1, 3, 4, 6, 10\}$ . The tested model parameters were justified from the literature on model calibration [32, 8, 1, 26]. We considered relative errors normalized by the reference prices to compare the methods. The statistical error of RQMC is defined as in (2.5), and the relative statistical error is given by

$$\text{Relative Statistical Error} = \frac{\text{Statistical Error}}{\text{Reference Value}},$$

where the reference values are computed using the MC method with  $M = 10^9$  samples. The numerical results were obtained using Google Colab with the standard configuration. The code containing the implementation of our proposed approach is available on GitHub<sup>3</sup>.

Through various tested examples, Section 4.1 demonstrates the sensitivity of the convergence of the QMC method to the choice of parameters in the domain transformation. Section 4.2 compares the proposed approach with employing the MC method in the Fourier domain. Then, Section 4.3 demonstrates that RQMC, with a suitable domain transformation, achieves substantial computational gains over the MC method in the physical domain for various dimensions and parameter combinations. Finally, Section 4.4 reveals that the RQMC applied in the Fourier space performs significantly better than the TP quadrature in the Fourier space and the MC method in the physical domain for options with up to 15 assets.

### 4.1 Effect of Domain Transformation on RQMC Convergence

This section illustrates the effect of the parameters of the distribution proposed for the domain transformation in Section 3 on the convergence of the RQMC method for put options in 1D under

<sup>3</sup><https://github.com/Michael-Samet/Quasi-Monte-Carlo-for-Efficient-Fourier-Pricing>

the GBM, VG, and NIG models. Figures 4.1a, 4.2a, 4.3a, and 4.4a demonstrate that the values of the parameters that do not satisfy the boundary growth conditions presented in Table 3.3 lead to integrands unbounded near the boundary of  $[0, 1]$ . Moreover, Figures 4.1b, 4.2b, 4.3b, and 4.4b demonstrate that these singular integrands exhibit much slower convergence rates of the QMC method. For instance, Figure 4.1a indicates that, for the GBM model, when the boundary growth condition is violated (i.e.,  $\tilde{\sigma} = 1 < \frac{1}{\sqrt{T}\sigma} = 5$ ), the integrand  $\tilde{g}(u)$  increases considerably near the boundary, and the associated convergence of RQMC deteriorates. This case is interesting because the choice of  $\tilde{\sigma} = 1$  is typical in the literature (e.g., in [2]). The parameter  $\tilde{\sigma}$  does not carry a physical significance; thus, the transformation is usually performed using the standard normal distribution, which adversely affects the convergence. The corresponding error is two magnitudes larger than the error obtained by RQMC when the parameter  $\tilde{\sigma}$  satisfies the boundary growth condition. In addition, Figures 4.3b, 4.3b visualize the considerable influence of the choice of both parameters,  $\tilde{\nu}$  and  $\tilde{\sigma}$ , on the convergence of RQMC in the VG model. These results motivate the use of the generalized Student's  $t$ -distribution instead of its standard counterpart in which the scaling parameter is fixed to  $\tilde{\sigma} = 1$ . Finally, Figure 4.2b illustrates that, for the NIG model, the error of RQMC is about three orders of magnitude lower if the domain transformation parameters are chosen appropriately, according to the procedure proposed in Section 3.2.3.

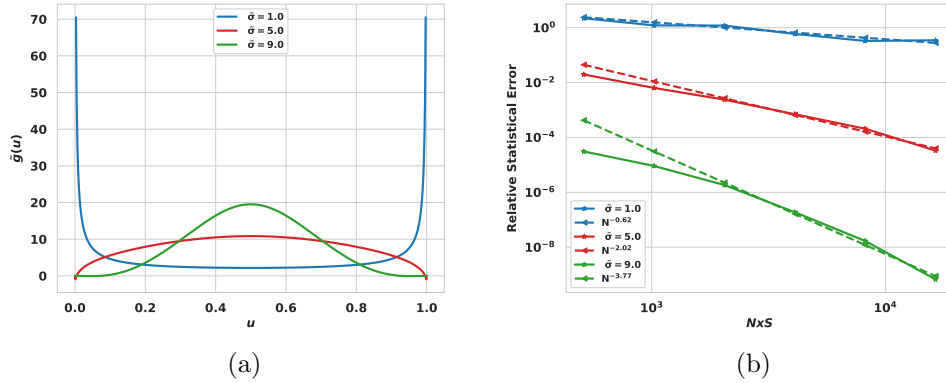


Figure 4.1: Effect of the parameter  $\tilde{\sigma}$  on (a) the shape of the transformed integrand  $\tilde{g}(u)$  and (b) convergence of the relative statistical error of RQMC with  $S_0 = 100$ ,  $K = 100$ ,  $r = 0$ ,  $T = 1$ , and  $\sigma = 0.2$  for a one-dimensional call option under the GBM model.  $N$ : number of QMC points;  $S = 32$ : number of digital shifts. Boundary growth condition limit:  $\bar{\sigma} = \frac{1}{\sqrt{T}\sigma} = 5$ .

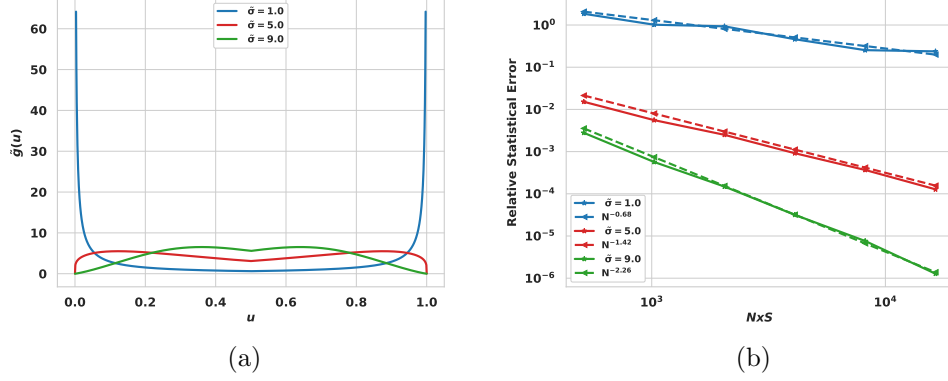


Figure 4.2: Effect of the parameter  $\tilde{\sigma}$  on (a) the shape of the transformed integrand  $\tilde{g}(u)$  and (b) convergence of the relative statistical error of RQMC with  $S_0 = 100$ ,  $K = 100$ ,  $r = 0$ ,  $T = 1$ ,  $\alpha = 20$ ,  $\beta = -3$ , and  $\delta = 0.2$  for a one-dimensional call option under the NIG model.  $N$ : number of QMC points;  $S = 32$ : number of digital shifts. Boundary growth condition limit:  $\bar{\sigma} = \frac{1}{T\delta} = 5$ .

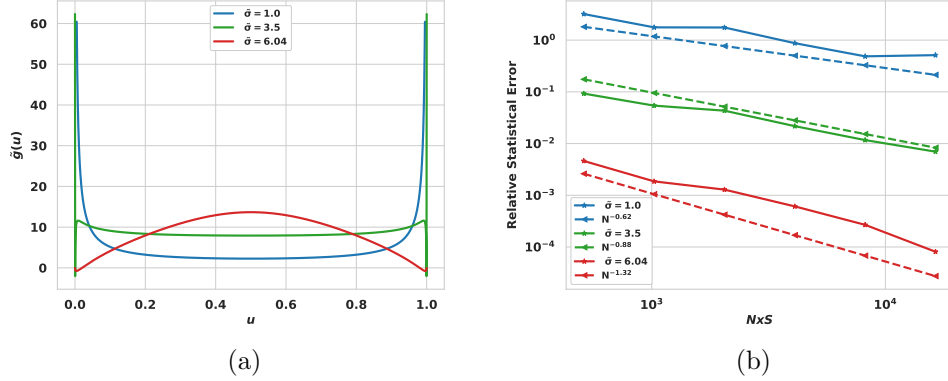


Figure 4.3: Effect of the parameter  $\tilde{\sigma}$  on (a) the shape of the transformed integrand  $\tilde{g}(u)$  and (b) convergence of the RQMC error for a one-dimensional call option under the VG model with  $S_0 = 100$ ,  $K = 100$ ,  $r = 0$ ,  $T = 1$ ,  $\sigma = 0.2$ ,  $\theta = -0.3$ , and  $\nu = 0.1$ .  $N$ : number of QMC points;  $S = 32$ : number of digital shifts. For the domain transformation,  $\tilde{\nu} = \frac{2T}{\nu} - 1 = 19$ . The critical value for the domain transformation is  $\bar{\sigma} = \left[ \frac{\nu\sigma^2\tilde{\nu}}{2} \right]^{\frac{T}{\nu-2T}} (\tilde{\nu})^{\frac{\nu}{4T-2\nu}} = 6.04$ .

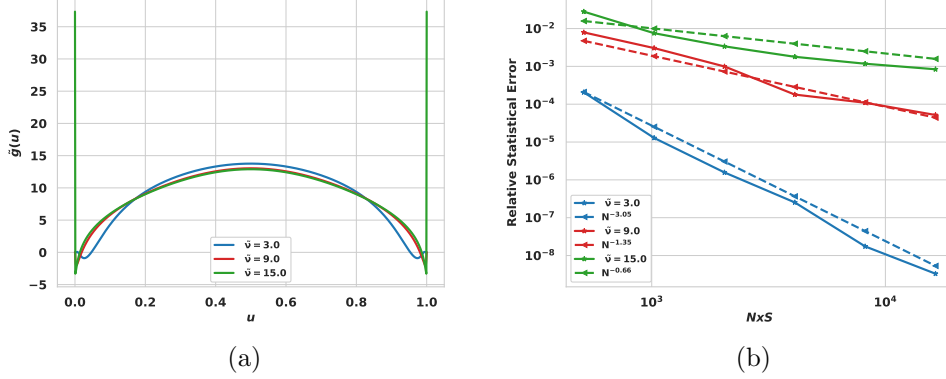


Figure 4.4: Effect of the parameter  $\tilde{\nu}$  on (a) the shape of the transformed integrand  $\tilde{g}(u)$  and (b) convergence of the RQMC error for a one-dimensional call option under the VG model with  $S_0 = 100$ ,  $K = 100$ ,  $r = 0$ ,  $T = 1$ ,  $\sigma = 0.2$ ,  $\theta = -0.3$ , and  $\nu = 0.2$ .  $N$ : number of QMC points;  $S = 32$ : number of digital shifts. For the domain transformation,  $\tilde{\sigma} = \left[ \frac{\nu\sigma^2\tilde{\nu}}{2} \right]^{\frac{T}{\nu-2T}} (\tilde{\nu})^{\frac{\nu}{4T-2\nu}}$  for each value of  $\tilde{\nu}$ . The critical value for the domain transformation is  $\bar{\nu} = \frac{2T}{\nu} - 1 = 9$ .

## 4.2 Comparison of the Proposed Approach with the Monte Carlo Method in the Fourier Space

This section demonstrates the advantage of employing QMC in the Fourier space over applying the MC method in the Fourier space, as in [2]. Although the MC method does not require a domain transformation, we must still introduce a density from which to sample. The MC estimator in the Fourier space is given by

$$\begin{aligned}
 V(\Theta_m, \Theta_p) &= \int_{\mathbb{R}^d} \frac{g(\mathbf{y})}{\prod_{j=1}^d \psi_j(y_j)} \prod_{j=1}^d \psi_j(y_j) d\mathbf{y} \\
 (4.1) \quad &\approx \frac{1}{N} \sum_{i=1}^N \frac{g(\Psi^{-1}(u_1(\omega_i)), \dots, \Psi^{-1}(u_d(\omega_i)))}{\prod_{j=1}^d \psi_j(\Psi^{-1}(u_j(\omega_i)))},
 \end{aligned}$$

where  $u_1(\omega_i), \dots, u_d(\omega_i)$  are sampled independently from the uniform distribution,  $\mathcal{U}([0, 1])$ ,  $\forall i = 1, \dots, N$ . The choice of the density,  $\psi(\cdot)$ , is the same for RQMC and MC for fairness of comparison. Table 3.3 provides additional details. The following numerical experiments demonstrate that applying RQMC with the appropriate domain transformation allows retaining nearly optimal convergence rates, in contrast to the MC method, in which the convergence rate is insensitive to the regularity of the integrand. Figures 4.5a, 4.5b, and 4.5c illustrate that employing RQMC in the Fourier space achieves a relative statistical error of about one order of magnitude lower than that of MC in the Fourier space. Moreover, the convergence rates of RQMC for the pricing of 4D basket put options are between  $\mathcal{O}(N^{-1})$  and  $\mathcal{O}(N^{-1.3})$ , which is double the rate  $\mathcal{O}(N^{-0.5})$  of the method. These optimal rates indicate that the RQMC method takes advantage of the analyticity of the integrand in the Fourier domain

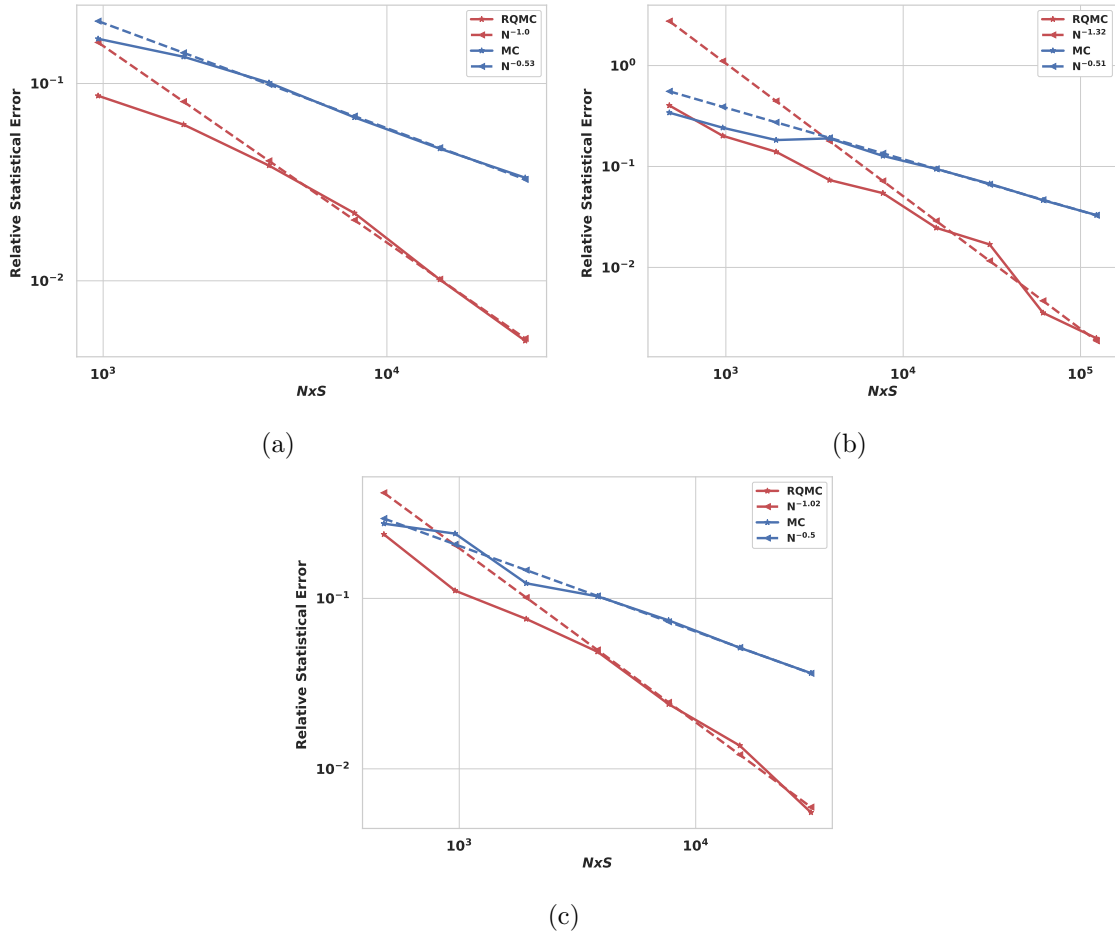


Figure 4.5: 4D basket put: convergence of the relative statistical error with respect to  $N \times S$  function evaluations. For RQMC,  $N$ : number of QMC points;  $S = 30$ : number of independent and identically distributed uniform shifts. For MC,  $N \times S$ : number of random samples in the approximation.  $S_0^j = 100$ ,  $K = 100$ ,  $r = 0$ , and  $T = 1$ . (a) GBM model:  $\sigma_j = 0.2$ ,  $\Sigma = \mathbf{I}_d$ ,  $\bar{\mathbf{R}}_j = 4.44$ ,  $\tilde{\sigma}_j = \frac{1}{\sqrt{T}\sigma} = 5$ . (b) VG model:  $\sigma_j = 0.4$ ,  $\theta_j = -0.3$ ,  $\nu = 0.2$ ,  $\Sigma = \mathbf{I}_d$ ,  $\bar{\mathbf{R}}_j = 1.31$ ,  $\tilde{\nu} = \frac{2T}{\nu} - 1 = 9$ ,  $\tilde{\sigma}_j = \left[ \frac{\nu\sigma_j^2\tilde{\nu}}{2} \right]^{\frac{T}{\nu-2T}} (\tilde{\nu})^{\frac{\nu}{4T-2\nu}} = 3.31$ . (c) NIG model:  $\alpha = 20$ ,  $\beta_j = -3$ ,  $\delta = 0.2$ ,  $\Delta = \mathbf{I}_d$ ,  $\bar{\mathbf{R}}_j = 5.73$ ,  $\forall j = 1, \dots, 4$ , and the domain transformation parameters are  $\tilde{\sigma}_j = \frac{1}{T\delta} = 10$ .

### 4.3 Computational Comparison of the Proposed Approach with the MC method in the Physical Space

This section demonstrates the advantage of the RQMC method in the Fourier space compared to the MC method in the physical space when the domain transformation from  $\mathbb{R}^d$  to  $[0, 1]^d$  is appropriately performed as proposed in Section 3.2. Figures 4.6b, 4.7b, and 4.8b reveal that the proposed approach outperforms the MC methods for options with up to six assets for the “call on min” options under all considered pricing models, with a factor of speedup of about 100. Figures 4.6a, 4.7a, and 4.8a reveal that RQMC may not be as advantageous as the MC method in

the case of basket put options if the desired relative tolerance is of order  $TOL = 10^{-2}$ . However, the RQMC method converges faster to deeper relative tolerance levels, such as  $TOL = 10^{-3}$ , because its rate of convergence is  $\mathcal{O}(TOL^{-1})$  compared to  $\mathcal{O}(TOL^{-2})$  for the MC method.

We conclude that the computational gains are more pronounced in the case of the call on min options, which is expected because the payoff function in the physical space of the call on min options is more irregular than the payoff function for the basket put option. Moreover, the performance of the MC method deteriorates more with the dimensions for the call on min options compared to the basket put options.

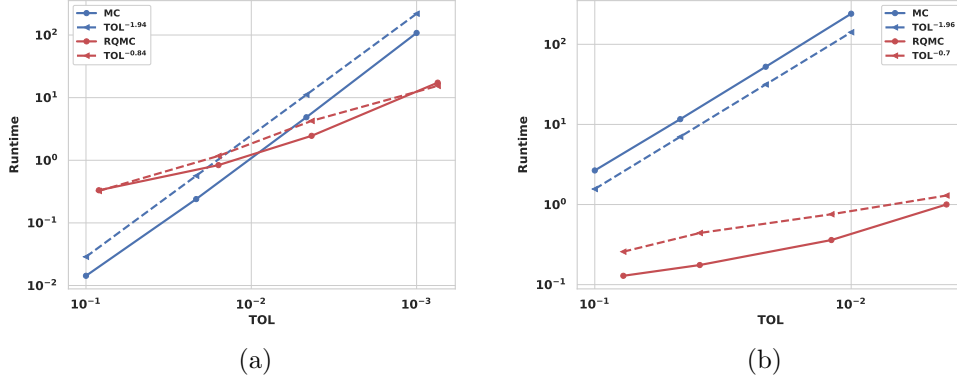


Figure 4.6: GBM: Average runtime in seconds with respect to relative tolerance levels  $TOL$  for (a) a four-dimensional basket put with  $\bar{\mathbf{R}}_j = 2.24$  and (b) six-dimensional call on min option with  $\bar{\mathbf{R}}_j = -2.97$  for  $S_0^j = 100$ ,  $K = 100$ ,  $\sigma_j = 0.4$ ,  $\Sigma = \mathbf{I}_d$ ,  $r = 0$ , and  $T = 1$ ,  $\forall j = 1, \dots, d$ . The domain transformation parameters are  $\tilde{\sigma}_j = \frac{1}{\sqrt{T}\sigma} = 2.5$

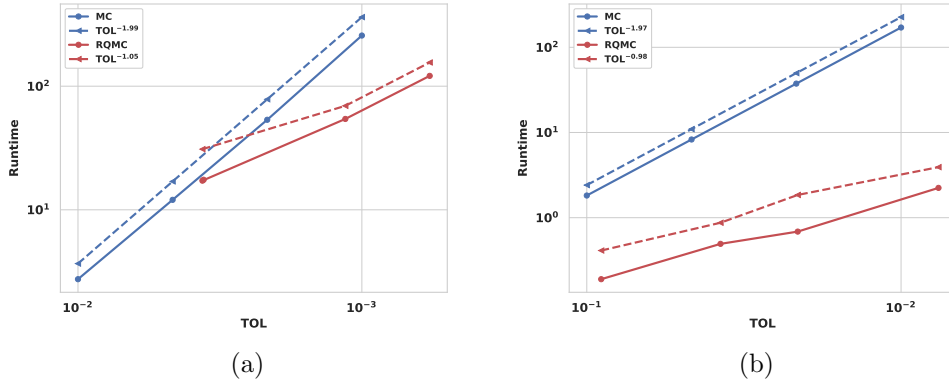


Figure 4.7: VG: Average runtime in seconds with respect to relative tolerance levels  $TOL$  for (a) the three-dimensional basket put with  $\bar{\mathbf{R}}_j = 1.5$  and (b) six-dimensional call on min option with  $\bar{\mathbf{R}}_j = -3.1$  for  $S_0^j = 100$ ,  $K = 100$ ,  $\sigma_j = 0.4$ ,  $\theta_j = -0.3$ ,  $\nu = 0.2$ ,  $\Sigma = \mathbf{I}_d$ ,  $r = 0$ , and  $T = 1$ ,  $\forall j = 1, \dots, d$ . The domain transformation parameters are  $\tilde{\nu} = \frac{2T}{\nu} - 1 = 9$  and  $\tilde{\sigma}_j = \sqrt{\frac{2}{\nu\tilde{\nu}\sigma_j^2}} = 3.31$ .

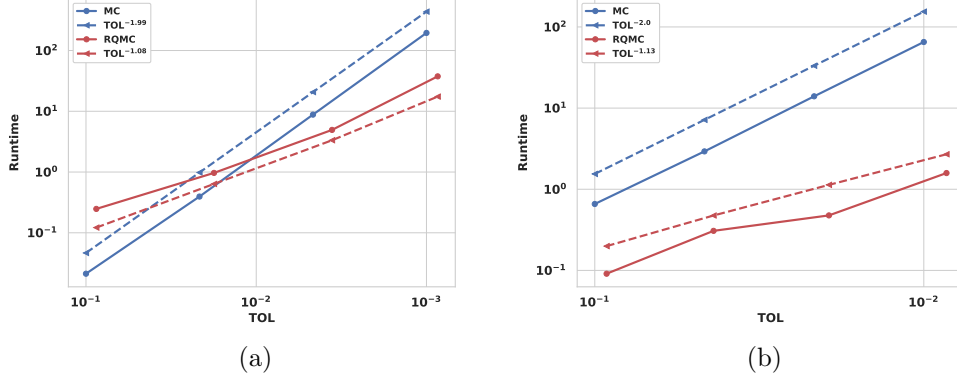


Figure 4.8: NIG: Average runtime in seconds with respect to relative tolerance levels  $TOL$  for (a) the six-dimensional basket put with  $\bar{\mathbf{R}}_j = 2.9$  and (b) six-dimensional call on min option with  $\bar{\mathbf{R}}_j = -8.08$  for  $S_0^j = 100$ ,  $K = 100$ ,  $\alpha = 15$ ,  $\beta_j = -3$ ,  $\delta = 0.2$ ,  $\Delta = \mathbf{I}_d$ ,  $r = 0$ , and  $T = 1$ ,  $\forall j = 1, \dots, d$ . The domain transformation parameter is  $\tilde{\sigma}_j = \frac{1}{T\delta} = 5$ .

#### 4.4 Runtime Comparison of RQMC with the MC and TP Quadratures

This section aims to compare the computational efficiency of the RQMC method with the commonly employed MC method in the physical space and the TP Gauss–Laguerre quadrature in the Fourier domain [61]. The runtime in Figures 4.9a, 4.9b, and 4.9c is the average time in seconds of seven runs for each of the methods to achieve a relative tolerance  $TOL = 10^{-2}$ . For the TP approach, only central processing unit (CPU) times of up to six dimensions are measured in Python, and the values for the remaining dimensions are numerically extrapolated. For the MC and RQMC methods, the criterion for error convergence is the relative statistical error. In contrast, for the TP quadrature, the stopping criterion is based on the exact relative error. The exact relative error is defined as the normalized absolute difference between the TP quadrature estimate and reference value computed using the MC method with  $M = 10^9$  samples. Consequently, the statistical error of the MC and RQMC methods is an upper bound; thus, the CPU times for the MC and RQMC methods are conservative because, in practice, they converge faster with respect to the exact relative error. Figures 4.9a, 4.9b, and 4.9c illustrate that the RQMC method applied in the Fourier space alleviates the curse of dimensionality, in contrast to the TP quadrature rule for which the cost grows exponentially with the dimensions. If the contour of integration is appropriately chosen and the domain transformation is handled carefully based on the proposed approach, the RQMC method significantly outperforms the MC method and TP quadrature for options with up to 15 underlying assets for the GBM, VG, and NIG models. In addition, although the convergence rate of the MC method is dimension-independent, the implied error constant increases with the dimensions. As a result, the RQMC approach reaches the target relative tolerance about 100 times faster than the MC method.

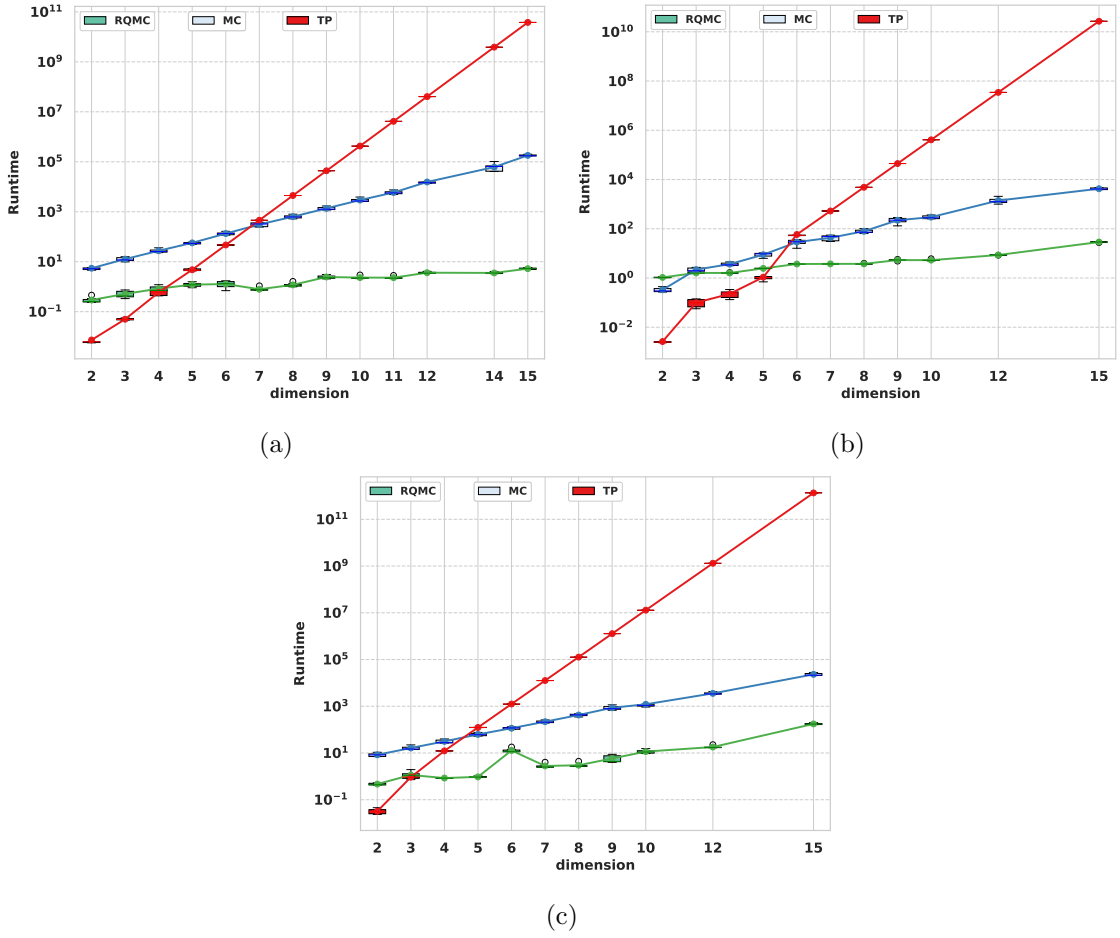


Figure 4.9: Runtime in seconds of the RQMC and TP quadrature in Fourier space and the MC method in direct space to reach a relative error,  $TOL = 10^{-2}$ , with respect to the dimensions for the call on min payoff with  $K = 100$ ,  $r = 0$ ,  $T = 1$ , and  $S_0^j = 100$ ,  $\forall j = 1, \dots, d$  under (a) the GBM model with  $\sigma_j = 0.2$ ,  $\Sigma = \mathbf{I}_d$ , and we use  $\tilde{\sigma}_j = \frac{1}{\sqrt{T}\sigma_j} = 5$  (b) VG model with  $\sigma_j = 0.4$ ,  $\theta_j = -0.3$ ,  $\nu = 0.1$ ,  $\Sigma = \mathbf{I}_d$ , and we use  $\tilde{\nu} = \frac{2T}{\nu} - 1 = 19$  and  $\tilde{\sigma}_j = \left[ \frac{\nu\sigma_j^2\tilde{\nu}}{2} \right]^{\frac{T}{\nu-2T}} (\tilde{\nu})^{\frac{\nu}{4T-2\nu}} = 2.91$ , and (c) NIG model with  $\alpha = 12$ ,  $\beta_j = -3$ ,  $\delta = 0.2$ ,  $\Delta = \mathbf{I}_d$ , and we use  $\tilde{\sigma}_j = \frac{\sqrt{2}}{T\delta} = 7.07$ . Both TP and RQMC quadratures use the optimal damping parameters as prescribed in [9]. The RQMC method employs  $S = 30$  digital shifts.

**Acknowledgments** C. Bayer gratefully acknowledges support from the German Research Foundation (DFG) via the Cluster of Excellence MATH+ (Project AA4-2). This publication is based on work supported by the King Abdullah University of Science and Technology (KAUST) Office of Sponsored Research (OSR) under Award No. OSR-2019-CRG8-4033 and the Alexander von Humboldt Foundation. Antonis Papapantoleon gratefully acknowledges the financial support from the Hellenic Foundation for Research and Innovation (Grant No. HFRI-FM17-2152).

**Declarations of Interest** The authors report no conflicts of interest. The authors alone are

responsible for the content and writing of the paper.

## References Cited

- [1] Jean-Philippe Aguilar. Some pricing tools for the variance Gamma model. *International Journal of Theoretical and Applied Finance*, 23(04):2050025, 2020.
- [2] L Ballotta. Powering up Fourier valuation to any dimension. *Wilmott*, 121:72–73, 2022.
- [3] Ole Barndorff-Nielsen. Exponentially decreasing distributions for the logarithm of particle size. *Proceedings of the Royal Society of London. A. Mathematical and Physical Sciences*, 353(1674):401–419, 1977.
- [4] Ole E Barndorff-Nielsen. Normal inverse Gaussian distributions and stochastic volatility modelling. *Scandinavian Journal of statistics*, 24(1):1–13, 1997.
- [5] Kinjal Basu and Art B Owen. Transformations and Hardy–Krause variation. *SIAM Journal on Numerical Analysis*, 54(3):1946–1966, 2016.
- [6] Christian Bayer, Chiheb Ben Hammouda, and Raúl Tempone. Hierarchical adaptive sparse grids and quasi-Monte Carlo for option pricing under the rough Bergomi model. *Quantitative Finance*, 20(9):1457–1473, 2020.
- [7] Christian Bayer, Chiheb Ben Hammouda, and Raúl Tempone. Numerical smoothing with hierarchical adaptive sparse grids and quasi-Monte Carlo methods for efficient option pricing. *Quantitative Finance*, 23(2):209–227, 2023.
- [8] Christian Bayer, Markus Siebenmorgen, and Raul Tempone. Smoothing the payoff for efficient computation of basket option prices. *Quantitative Finance*, 18(3):491–505, 2018.
- [9] A. Papapantoleon M. Samet C. Bayer, C. Ben Hammouda and R. Tempone. Optimal damping with hierarchical adaptive quadrature for efficient Fourier pricing of multi-asset options in Lévy models. *Journal of Computational Finance*, 27(3):43–86, 2024.
- [10] Peter Carr and Dilip Madan. Option valuation using the fast Fourier transform. *Journal of Computational Finance*, 2(4):61–73, 1999.
- [11] Gemma Colldeforns-Papiol, Luis Ortiz-Gracia, and Cornelis W Oosterlee. Two-dimensional Shannon wavelet inverse Fourier technique for pricing European options. *Applied Numerical Mathematics*, 117:115–138, 2017.
- [12] Andrew R Conn, Nicholas IM Gould, and Philippe L Toint. *Trust region methods*. SIAM, 2000.
- [13] Stefano Demarta and Alexander J McNeil. The t copula and related copulas. *International statistical review*, 73(1):111–129, 2005.
- [14] Josef Dick, Frances Y Kuo, and Ian H Sloan. High-dimensional integration: the quasi-Monte Carlo way. *Acta Numerica*, 22:133–288, 2013.

- [15] Daniel J Duffy. *Finite Difference methods in financial engineering: a Partial Differential Equation approach*. John Wiley & Sons, 2013.
- [16] Johannes Jisse Duistermaat and Lars Hormander. *Fourier integral operators*, volume 2. Springer, 1996.
- [17] Ernst Eberlein, Kathrin Glau, and Antonis Papapantoleon. Analysis of Fourier transform valuation formulas and applications. *Applied Mathematical Finance*, 17(3):211–240, 2010.
- [18] Fang Fang and Cornelis W. Oosterlee. A novel pricing method for European options based on Fourier-cosine series expansions. *SIAM Journal on Scientific Computing*, 31(2):826–848, 2008.
- [19] Liming Feng and Vadim Linetsky. Pricing options in jump-diffusion models: an extrapolation approach. *Operations Research*, 56(2):304–325, 2008.
- [20] Emmanuil Georgoulis, Antonis Papapantoleon, and Costas Smaragdakis. A deep implicit-explicit minimizing movement method for option pricing in jump-diffusion models, 01 2024.
- [21] Paul Glasserman. *Monte Carlo methods in financial engineering*, volume 53. Springer, 2004.
- [22] Kathrin Glau and Linus Wunderlich. The deep parametric pde method and applications to option pricing. *Applied Mathematics and Computation*, 432:127355, 2022.
- [23] Jiequn Han, Arnulf Jentzen, and Weinan E. Solving high-dimensional partial differential equations using deep learning. *Proceedings of the National Academy of Sciences*, 115(34):8505–8510, 2018.
- [24] Jürgen Hartinger, Reinhold Kainhofer, and Volker Ziegler. On the corner avoidance properties of various low-discrepancy sequences. *INTEGERS: Electronic Journal of Combinatorial Number Theory*, 5(3):A10, 2005.
- [25] Zhijian He, Zhan Zheng, and Xiaoqun Wang. On the error rate of importance sampling with randomized quasi-Monte Carlo. *SIAM Journal on Numerical Analysis*, 61(2):515–538, 2023.
- [26] Jherek Healy. The pricing of vanilla options with cash dividends as a classic vanilla basket option problem. *arXiv preprint arXiv:2106.12971*, 2021.
- [27] Edmund Hlawka. Funktionen von beschränkter variatiou in der theorie der gleichverteilung. *Annali di Matematica Pura ed Applicata*, 54(1):325–333, 1961.
- [28] Markus Holtz. *Sparse grid quadrature in high dimensions with applications in finance and insurance*, volume 77. Springer Science & Business Media, 2010.
- [29] Friedrich Hubalek and Jan Kallsen. Variance-optimal hedging and Markowitz-efficient portfolios for multivariate processes with stationary independent increments with and without constraints. Technical report, Working paper, TU München, 2005.
- [30] Thomas R Hurd and Zhuowei Zhou. A Fourier transform method for spread option pricing. *SIAM Journal on Financial Mathematics*, 1(1):142–157, 2010.

- [31] Michael Kastoryano and Nicola Pancotti. A highly efficient tensor network algorithm for multi-asset Fourier options pricing. *arXiv preprint arXiv:2203.02804*, 2022.
- [32] J. Lars. Kirkby. Efficient option pricing by frame duality with the fast Fourier transform. *SIAM Journal on Financial Mathematics*, 6(1):713–747, 2015.
- [33] Justin L Kirkby. *Frame and Fourier methods for exotic option pricing and hedging*. PhD thesis, Georgia Institute of Technology, 2016.
- [34] Samuel Kotz, Tomasz Kozubowski, and Krzysztof Podgórski. *The Laplace distribution and generalizations: a revisit with applications to communications, economics, engineering, and finance*. Number 183. Springer Science & Business Media, 2001.
- [35] Frances Y Kuo, Ch Schwab, and Ian H Sloan. Quasi-monte carlo methods for high-dimensional integration: the standard (weighted hilbert space) setting and beyond. *The ANZIAM Journal*, 53(1):1–37, 2011.
- [36] Frances Y Kuo, Ian H Sloan, Grzegorz W Wasilkowski, and Benjamin J Waterhouse. Randomly shifted lattice rules with the optimal rate of convergence for unbounded integrands. *Journal of Complexity*, 26(2):135–160, 2010.
- [37] Frances Y Kuo, Grzegorz W Wasilkowski, and Benjamin J Waterhouse. Randomly shifted lattice rules for unbounded integrands. *Journal of Complexity*, 22(5):630–651, 2006.
- [38] Gerhard Larcher, Harald Niederreiter, and Wolfgang Ch Schmid. Digital nets and sequences constructed over finite rings and their application to quasi-Monte Carlo integration. *Monatshefte für Mathematik*, 121:231–253, 1996.
- [39] Regis Lebrun and Anne Dutfoy. An innovating analysis of the Nataf transformation from the copula viewpoint. *Probabilistic Engineering Mechanics*, 24(3):312–320, 2009.
- [40] Pierre L’Ecuyer and Christiane Lemieux. Recent advances in randomized quasi-Monte Carlo methods. *Modeling uncertainty: An examination of stochastic theory, methods, and applications*, pages 419–474, 2002.
- [41] Levendorskii. Pitfalls of the Fourier transform method in affine models, and remedies.
- [42] Alan L. Lewis. A simple option formula for general jump-diffusion and other exponential Lévy processes. *Available at SSRN 282110*, 2001.
- [43] Yiou Li, Lulu Kang, and Fred J Hickernell. Is a transformed low discrepancy design also low discrepancy? *Contemporary Experimental Design, Multivariate Analysis and Data Mining: Festschrift in Honour of Professor Kai-Tai Fang*, pages 69–92, 2020.
- [44] Yang Liu and Raúl Tempone. Nonasymptotic convergence rate of quasi-Monte Carlo: Applications to linear elliptic pdes with lognormal coefficients and importance samplings. *arXiv preprint arXiv:2310.14351*, 2023.
- [45] Francis A Longstaff. Option pricing and the martingale restriction. *The Review of Financial Studies*, 8(4):1091–1124, 1995.

- [46] Roger Lord and Christian Kahl. Optimal Fourier inversion in semi-analytical option pricing. 2007.
- [47] Elisa Luciano and Wim Schoutens. A multivariate jump-driven financial asset model. *Quantitative finance*, 6(5):385–402, 2006.
- [48] Roger B Nelsen. *An introduction to copulas*. Springer, 2006.
- [49] James A Nichols and Frances Y Kuo. Fast CBC construction of randomly shifted lattice rules achieving  $O(n^{-1+\delta})$  convergence for unbounded integrands over  $\mathbb{R}^s$  in weighted spaces with POD weights. *Journal of Complexity*, 30(4):444–468, 2014.
- [50] Du Ouyang, Xiaoqun Wang, and Zhijian He. Quasi-monte carlo for unbounded integrands with importance sampling. *arXiv preprint arXiv:2310.00650*, 2023.
- [51] Art B Owen. Multidimensional variation for quasi-Monte Carlo. In *Contemporary Multivariate Analysis And Design Of Experiments: In Celebration of Professor Kai-Tai Fang’s 65th Birthday*, pages 49–74. World Scientific, 2005.
- [52] Art B Owen. Halton sequences avoid the origin. *SIAM review*, 48(3):487–503, 2006.
- [53] Radha Panini. *Option pricing with Mellin transforms*. State University of New York at Stony Brook, 2004.
- [54] Sebastian Raible. *Lévy processes in finance: Theory, numerics, and empirical facts*. PhD thesis, Universität Freiburg i. Br, 2000.
- [55] Murray Rosenblatt. Remarks on a multivariate transformation. *The annals of mathematical statistics*, 23(3):470–472, 1952.
- [56] Marjon J Ruijter and Cornelis. W. Oosterlee. Two-dimensional Fourier cosine series expansion method for pricing financial options. *SIAM Journal on Scientific Computing*, 34(5):B642–B671, 2012.
- [57] Ilya M Sobol’, Danil Asotsky, Alexander Kreinin, and Sergei Kucherenko. Construction and comparison of high-dimensional Sobol’generators. *Wilmott*, 2011(56):64–79, 2011.
- [58] Edward C Titchmarsh. Introduction to the theory of Fourier integrals. 1948.
- [59] Lina von Sydow, Lars Josef Höök, Elisabeth Larsson, Erik Lindström, Slobodan Milovanović, Jonas Persson, Victor Shcherbakov, Yuri Shpolyanskiy, Samuel Sirén, Jari Toivanen, et al. Benchop—the benchmarking project in option pricing. *International Journal of Computer Mathematics*, 92(12):2361–2379, 2015.
- [60] Song Wang. A novel fitted finite volume method for the Black–Scholes equation governing option pricing. *IMA Journal of Numerical Analysis*, 24(4):699–720, 2004.
- [61] Magnus Wiktorsson. Notes on the benchop implementations for the Fourier Gauss Laguerre FGL method, 2015.

- [62] Tien-Tsin Wong, Wai-Shing Luk, and Pheng-Ann Heng. Sampling with Hammersley and Halton points. *Journal of graphics tools*, 2(2):9–24, 1997.
- [63] Ye Xiao and Xiaoqun Wang. Conditional quasi-Monte Carlo methods and dimension reduction for option pricing and hedging with discontinuous functions. *Journal of Computational and Applied Mathematics*, 343:289–308, 2018.
- [64] Ciyou Zhu, Richard H Byrd, Peihuang Lu, and Jorge Nocedal. Algorithm 778: L-BFGS-B: Fortran subroutines for large-scale bound-constrained optimization. *ACM Transactions on mathematical software (TOMS)*, 23(4):550–560, 1997.

## A Pricing Models

For the asset dynamics in this work, we studied three models given by Examples A.1, A.2, and A.3.

**Example A.1** (Multivariate Geometric Brownian Motion (GBM)). The joint risk-neutral dynamics of the stock prices are modeled as follows:<sup>4</sup>

$$(A.1) \quad S_i(t) \stackrel{\mathbb{Q}}{=} S_i(0) \exp \left[ \left( r - \frac{\sigma_i^2}{2} \right) t + \sigma_i W_i(t) \right], \quad i = 1, \dots, d,$$

where  $\sigma_1, \dots, \sigma_d > 0$  and  $\{W_1(t), \dots, W_d(t), t \geq 0\}$  are correlated standard Brownian motions, where  $-1 \leq \rho_{i,j} \leq 1$  denotes the correlation between  $W_i$  and  $W_j$ . Moreover,  $\Sigma \in \mathbb{R}^{d \times d}$  denotes the covariance matrix of the log returns  $\{\log(\frac{S_i(t)}{S_i(0)})\}_{i=1}^d$ , where  $\Sigma_{ij} = \rho_{i,j} \sigma_i \sigma_j$ .

**Example A.2** (Multivariate Variance Gamma (VG) [47]). The joint risk-neutral dynamics of the stock prices are modeled as follows:

$$(A.2) \quad S_i(t) \stackrel{\mathbb{Q}}{=} S_i(0) \exp \left\{ (r + \mu_{VG,i}) t + \theta_i G(t) + \sigma_i \sqrt{G(t)} W_i(t) \right\}, \quad i = 1, \dots, d,$$

where  $\{W_1(t), \dots, W_d(t)\}$  denote independent standard Brownian motions, and  $\{G(t)|t \geq 0\}$  is a common gamma process with parameters  $(\frac{t}{\nu}, \frac{1}{\nu})$  and is independent of all Brownian motion. Additionally,  $\theta_i \in \mathbb{R}$  and  $\sigma_i > 0$ , where  $1 \leq i \leq d$ . The covariance matrix  $\Sigma \in \mathbb{R}^{d \times d}$  satisfies  $\Sigma_{i,j} = \sigma_i^2$  for  $i = j$  and is zero otherwise. Finally,  $\mu_{VG} := (\mu_{VG,1}, \dots, \mu_{VG,d})$  represent the martingale correction terms that ensure that  $\{e^{-rt} S_i(t)|t \geq 0\}$  is a martingale. These terms are given by

$$(A.3) \quad \mu_{VG,i} = \frac{1}{\nu} \log \left( 1 - \frac{1}{2} \sigma_i^2 \nu - \theta_i \nu \right), \quad i = 1, \dots, d.$$

**Example A.3** (Multivariate Normal Inverse Gaussian (NIG) [4, 3]). The joint risk-neutral dynamics of the stock prices are modeled as follows:

$$(A.4) \quad S_i(t) \stackrel{\mathbb{Q}}{=} S_i(0) \exp \left\{ (r + \mu_{NIG,i}) t + \beta_i IG(t) + \sqrt{IG(t)} W_i(t) \right\}, \quad i = 1, \dots, d,$$

---

<sup>4</sup> $\stackrel{\mathbb{Q}}{=}$  denotes the equality with respect to the risk-neutral distribution  $\mathbb{Q}$ .

where  $\{W_1(t), \dots, W_d(t)\}$  denotes independent standard Brownian motion, and  $\{IG(t)|t \geq 0\}$  is a common inverse Gaussian process with parameters  $(\delta^2 t^2, \alpha^2 - \boldsymbol{\beta}^T \boldsymbol{\Delta} \boldsymbol{\beta})$  and is independent of all Brownian motion. Additionally,  $\alpha \in \mathbb{R}_+$ ,  $\boldsymbol{\beta} \in \mathbb{R}^d$ ,  $\alpha^2 > \boldsymbol{\beta}^T \boldsymbol{\Delta} \boldsymbol{\beta}$ ,  $\delta > 0$ , and  $\boldsymbol{\Delta} \in \mathbb{R}^{d \times d}$  is a symmetric positive definite matrix with a unit determinant. Moreover,  $\{\mu_{NIG,i}\}_{i=1}^d$  denotes martingale correction terms that ensure that  $\{e^{-rt} S_i(t)|t \geq 0\}$  is a martingale, given by

$$(A.5) \quad \mu_{NIG,i} = -\delta \left( \sqrt{\alpha^2 - \beta_i^2} - \sqrt{\alpha^2 - (\beta_i + 1)^2} \right), \quad i = 1, \dots, d.$$

## B Proof of Proposition 3.3

In the first step, we simply multiply and divide the original integrand by  $\psi_{stu}(\cdot)$

$$(B.1) \quad \int_{\mathbb{R}^d} g(\mathbf{y}) d\mathbf{y} = \int_{\mathbb{R}^d} \bar{g}(\mathbf{y}) \psi_{stu}(\mathbf{y}) d\mathbf{y},$$

where  $\bar{g}(\mathbf{y}) = \frac{g(\mathbf{y})}{\psi_{stu}(\mathbf{y})}$ . We let  $\mathbf{T} \sim t_d(\mathbf{0}, \tilde{\boldsymbol{\Sigma}}, \tilde{\nu})$ ,  $\mathbf{Z} \sim \mathcal{N}_d(\mathbf{0}, \tilde{\boldsymbol{\Sigma}})$  and  $W \sim \chi^2(\tilde{\nu})$ , independent of  $\mathbf{Z}$ . Then, we use the following representation of the multivariate t distribution [13]

$$(B.2) \quad \mathbf{T} \stackrel{d}{=} \mathbf{Z} \sqrt{\frac{\tilde{\nu}}{W}}.$$

For notational convenience, we define the scaled multivariate normal distribution by  $\tilde{\mathbf{Z}} := \sqrt{\tilde{\nu}} \times \mathbf{Z}$ , and we note that  $\sqrt{W}$  follows the chi distribution with degrees of freedom  $\tilde{\nu}$ . The random vector  $\mathbf{T}$  is now given as a ratio of two independent RVs (i.e.,  $\mathbf{T} = \frac{\tilde{\mathbf{Z}}}{\sqrt{W}}$ ); thus, its PDF can be expressed as follows:

$$(B.3) \quad \psi_{stu}(\mathbf{y}) = \int_0^{+\infty} w^d \psi_{\tilde{\mathbf{Z}}}(w\mathbf{y}) \psi_{chi}(w) dw, \quad \mathbf{y} \in \mathbb{R}^d.$$

Inserting the new expression of the PDF of the multivariate Student's  $t$ -distribution in the original integrand and using Fubini's theorem results in the following:

$$(B.4) \quad \begin{aligned} \int_{\mathbb{R}^d} \bar{g}(\mathbf{y}) \psi_{stu}(\mathbf{y}) d\mathbf{y} &= \int_{\mathbb{R}^d} \bar{g}(\mathbf{y}) \left( \int_0^{+\infty} w^d \psi_{\tilde{\mathbf{Z}}}(w\mathbf{y}) \psi_{chi}(w) dw \right) d\mathbf{y} \\ &= \int_0^{+\infty} w^d \left( \int_{\mathbb{R}^d} \bar{g}(\mathbf{y}) \psi_{\tilde{\mathbf{Z}}}(w\mathbf{y}) d\mathbf{y} \right) \psi_{chi}(w) dw \\ &= \int_0^{+\infty} \left( \int_{\mathbb{R}^d} \bar{g}\left(\frac{\mathbf{y}}{w}\right) \psi_{\tilde{\mathbf{Z}}}(\mathbf{y}) d\mathbf{y} \right) \psi_{chi}(w) dw \\ &= \int_0^{+\infty} \left( \int_{[0,1]^d} \bar{g}\left(\frac{\Psi_{\tilde{\mathbf{Z}}}^{-1}(\mathbf{u})}{w}\right) d\mathbf{u} \right) \psi_{chi}(w) dw. \\ &= \int_0^{+\infty} \left( \int_{[0,1]^d} \bar{g}\left(\tilde{\mathbf{L}} \cdot \frac{\Psi_{nor}^{-1}(\mathbf{u}; \mathbf{I}_d)}{w}\right) \psi_{chi}(w) d\mathbf{u} \right) dw. \end{aligned}$$

## C Proof of Proposition 3.5

In the first step, we simply multiply and divide the original integrand by  $\psi_{lap}(\cdot)$

$$(C.1) \quad \int_{\mathbb{R}^d} g(\mathbf{y}) d\mathbf{y} = \int_{\mathbb{R}^d} \bar{g}(\mathbf{y}) \psi_{lap}(\mathbf{y}) d\mathbf{y},$$

where  $\bar{g}(\mathbf{y}) = \frac{g(\mathbf{y})}{\psi_{lap}(\mathbf{y})}$ . We let  $\mathbf{Y} \sim \mathbf{ML}_d(\mathbf{0}, \tilde{\Sigma})$ ,  $\mathbf{Z} \sim \mathcal{N}_d(\mathbf{0}, \tilde{\Sigma})$  and  $W \sim \exp(1)$ , independent of  $\mathbf{Z}$ . Thus, by Theorem 6.3.1 in [34], we have that

$$(C.2) \quad \mathbf{Y} \stackrel{d}{=} \sqrt{W} \mathbf{Z}.$$

We note that  $\sqrt{W} \sim \text{Rayleigh}(\frac{1}{\sqrt{2}})$  follows the Rayleigh distribution with scale parameter  $\frac{1}{\sqrt{2}}$ . The random vector  $\mathbf{Y}$  is now the product of two independent RVs; hence, its PDF can be expressed as

$$(C.3) \quad \psi_{lap}(\mathbf{y}) = \int_0^{+\infty} (w)^{-d} \psi_{\mathbf{Z}}\left(\frac{\mathbf{y}}{w}\right) \psi_{ray}(w) dw, \mathbf{y} \in \mathbb{R}^d.$$

Inserting the new expression of the PDF of the multivariate Laplace distribution (C.3) in the expression of the original integrand and using Fubini's theorem provides the following result:

$$(C.4) \quad \begin{aligned} \int_{\mathbb{R}^d} \bar{g}(\mathbf{y}) \psi_{lap}(\mathbf{y}) d\mathbf{y} &= \int_{\mathbb{R}^d} \bar{g}(\mathbf{y}) \left( \int_0^{+\infty} (w)^{-d} \psi_{\mathbf{Z}}\left(\frac{\mathbf{y}}{w}\right) \psi_{ray}(w) dw \right) d\mathbf{y} \\ &= \int_0^{+\infty} (w)^{-d} \left( \int_{\mathbb{R}^d} \bar{g}(\mathbf{y}) \psi_{\mathbf{Z}}\left(\frac{\mathbf{y}}{w}\right) d\mathbf{y} \right) \psi_{ray}(w) dw \\ &= \int_0^{+\infty} \left( \int_{\mathbb{R}^d} \bar{g}(w\mathbf{y}) \psi_{\mathbf{Z}}(\mathbf{y}) d\mathbf{y} \right) \psi_{ray}(w) dw \\ &= \int_0^{+\infty} \left( \int_{[0,1]^d} \bar{g}(w\Psi_{\mathbf{Z}}^{-1}(\mathbf{u})) d\mathbf{u} \right) \psi_{ray}(w) dw. \end{aligned}$$